Dynamic switching of crotonylation to ubiquitination of H2A at lysine 119 attenuates transcription–replication conflicts caused by replication stress

Shuailin Hao[1], Ya Wang[1], Yuqin Zhao[1], Wen Gao[1], Wei Cui[1], Youhang Li[1], Jian Cui[1], Yu Liu[1], Lixiu Lin[1], Xingzhi Xu ⬤[2] and Hailong Wang ⬤[1,*]

[1]Beijing Key Laboratory of DNA Damage Response and College of Life Sciences, Capital Normal University, Beijing 100048, China and [2]Guangdong Key Laboratory for Genome Stability and Disease Prevention and Carson International Cancer Center, Marshall Laboratory of Biomedical Engineering, China Shenzhen University School of Medicine, Shenzhen, Guangdong 518060, China

ABSTRACT

The reversible post-translational modification (PTM) of proteins plays an important role in many cellular processes. Lysine crotonylation (Kcr) is a newly identified PTM, but its functional significance remains unclear. Here, we found that Kcr is involved in the replication stress response. We show that crotonylation of histone H2A at lysine 119 (H2AK119) and ubiquitination of H2AK119 are reversibly regulated by replication stress. Decrotonylation of H2AK119 by SIRT1 is a prerequisite for subsequent ubiquitination of H2AK119 by BMI1. Accumulation of ubiquitinated H2AK119 at reversed replication forks leads to the release of RNA Polymerase II and transcription repression in the vicinity of stalled replication forks. These effects attenuate transcription–replication conflicts (TRCs) and TRC-associated R-loop formation and DNA double-strand breaks. These findings suggest that decrotonylation and ubiquitination of H2A at lysine 119 act together to resolve replication stress-induced TRCs and protect genome stability.

GRAPHICAL ABSTRACT
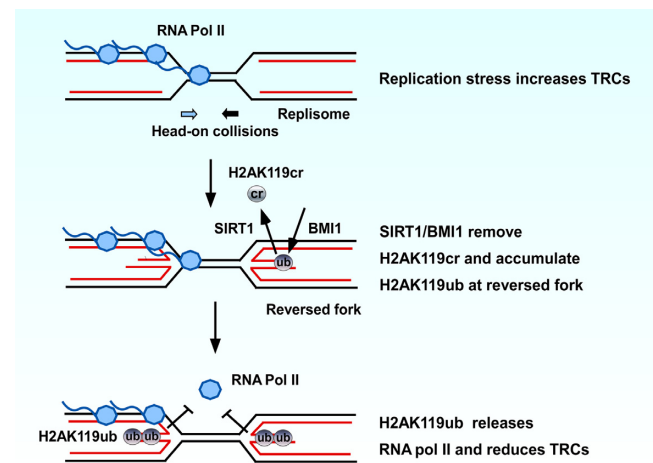
INTRODUCTION

Cells are subject to constant external and internal genotoxic stresses that threaten the stability and integrity of the genome. In response to these insults, cells invoke elaborate mechanisms collectively known as the DNA damage response (DDR) to maintain genomic stability (1,2). The DDR is a concerted process that can detect and repair DNA damage, regulate the cell cycle and transcription and determine cell fate. The cellular networks involved in the DDR include many proteins and post-translational modifications (PTMs), which work in a coordinated manner to counteract various genotoxic stresses. Defects in DDR systems can lead to cancer-prone inherited syndromes, such as ataxia–telangiectasia, Nijmegen breakage syndrome and Fanconi anemia (1–6).

*To whom correspondence should be addressed. Tel: +86 10 68901494; Fax: +86 10 68902440; Email: Hailwang@cnu.edu.cn

In recent years, high-sensitivity mass spectrometry (MS) has helped identify several novel histone short-chain lysine acylation modifications, including propionylation, butyrylation, 2-hydroxyisobutyrylation, succinylation, malonylation, glutarylation, crotonylation, β-hydroxybutyrylation and lactylation. These modifications are distinct in hydrocarbon chain length, hydrophobicity or charge, but they are structurally similar to the well-studied lysine acetylation (7–15). To date, very little is known about the functional significance of these newly identified PTMs. Lysine crotonylation (Kcr) was first discovered about 10 years ago, as a PTM of histone (13). Subsequently, it was revealed that Kcr is an evolutionarily conserved and common PTM that occurs in both core histone and some non-histone proteins in a variety of organisms. Similar to other types of PTM, Kcr is a reversible modification. The classic histone acetyltransferases (HATs), p300/CBP, PCAF, and MOF, are responsible for most crotonylation events, while the histone deacetylases (HDACs) HDAC1/2/3 and SIRT1/2/3 reverse these reactions (16–21). The chromodomain protein CDYL acts as a crotonyl-CoA hydratase to negatively regulate histone Kcr by reducing substrate supply (22). CDYL-regulated Kcr of RPA1 plays an important role in homologous recombination (HR)-mediated DNA repair (23), while HDAC-regulated histone crotonylation is reduced after DNA damage (24). These findings show that Kcr is involved in the DDR.

RNA transcription shares the same DNA template as DNA replication, and thus conflicts between transcription and replication can occur as the result of collisions between the multi-enzyme machineries that catalyze these two processes. Uncoordinated transcription–replication conflicts (TRCs) may change the transcription process, create replication stress, induce stalling of DNA replication forks, and cause DNA recombination, DNA breaks and mutations (25–31). TRCs thus contribute to genome instability (32–35). During TRCs, DNA replication and transcription complexes can become closer to each other either in a head-on or co-directional orientation. It is generally thought that head-on collision leads to the formation of R-loops—structures containing a DNA–RNA hybrid—which can block replication and induce DNA damage and genome instability (26,27,30,31,36–42). In the human genome, replication forks are usually co-directional with the transcription complex. This co-directional bias allows cells to reduce the physiological levels of R-loops and avoid their harmful effects during unperturbed conditions (31,43). Upon replication stress, replication forks can stall, and dormant replication origins in the vicinity are activated to rescue stalled replication. In regions with actively expressed genes, replication stress-induced fork stalling and origin firing can increase the level of head-on TRCs and further exacerbate the threat to genomic stability (35,43,44). The molecular pathways and detailed mechanisms by which cells coordinate transcription and replication during replication stress remain unclear.

Transcription and replication both involve histone modifications, which modulate the accessibility of DNA as well as the recruitment of related enzymes or factors.

Histone H2A was the first ubiquitinated protein to be identified (45,46). Mono-ubiquitination of H2A on lysine 119 (H2AK119ub) correlates with transcriptional repression (47). H2AK119ub occurs locally at ultraviolet (UV)-induced lesions and DNA double-strand break (DSB) sites (48–52). H2AK119ub suppresses transcription at regions surrounding DSBs by removing the elongating RNA Polymerase II (RNA Pol II) from the transcribed template (53). To date, it is not clear whether H2AK119ub is also involved in other types of DDR, such as the replication stress-induced signaling pathway.

In this study, we found that H2AK119cr and H2AK119ub exist simultaneously in the cell and are reversibly regulated by replication stress. Crotonylation of H2AK119 is mediated by SIRT1 deacetylase and is a prerequisite for subsequent BMI1-mediated ubiquitination at this site. Enrichment of H2AK119ub at the reverse replication fork promotes the removal of RNA Pol II, suppresses transcription of genes located near the stalled replication forks, and reduces the formation of R-loops and DSBs. SIRT1-mediated H2AK119cr removal and BMI1-mediated H2AK119ub are important for resolving TRCs under replication stress.

MATERIALS AND METHODS

Cell culture, cell lines, antibodies and reagents

Human U2OS, HCT116, HeLa and 293T cells were cultured at 37°C in Dulbecco's modified Eagle's medium with 10% fetal bovine serum in the presence of antibiotics and 5% CO_2. SIRT1- and BMI1-knockout U2OS cells were generated using CRISPR–Cas9 technology. The following guide RNA (gRNA) sequences targeting the seventh exon of BMI1 and the third exon of SIRT1 were selected using an optimized CRISPR design tool (http://crispr.mit.edu; 54:): gRNA-BMI1: AACGTGTATTGTTCGTTACC, gRNA-SIRT1: TCAATATCAAACATCGCTTG.

Antibodies against FLAG (F1804) and anti-Myc (M4439) were purchased from Sigma. Anti-PanKcr (PTM-502) and anti-H2AK119cr (PTM-543) were purchased from PTM Biolabs. Anti-γH2AX (05–636) and anti-PCNA (3428716) were purchased from Millipore. Anti-SIRT1 (A300-688A), anti-BMI1 (A301-694A), and anti-RPA2 (A300-244A) were purchased from Bethyl. Anti-H2AK119ub (8240) anti-H2A (2578) and anti-ASF1a (2990) were purchased from Cell Signaling Technology. Anti-S9.6 (ENH001) was purchased from Kerafast. Anti-RNA Polymerase II (ab817) and anti-nucleolin (ab50279) were purchased from Abcam. Anti-BRCA1(D9) was purchased from Santa Cruz. Anti-biotin (200–002-211) was purchased from Jackson ImmunoResearch. Anti-IgA-allophycocyanin (559353) and fluorescein isothiocyanate (FITC)-conjugated anti-mouse IgM (17-5790) were purchased from Becton, Dickinson and Company. Etoposide (E1383), camptothecin (C9911), hydroxyurea (H8627), and aphidicolin (A4487) were purchased from Sigma. Doxorubicin (S1208) and trichostatin A (S1405) were purchased from Selleck. Nicotinamide (S1761) was purchased from Beyotime Biotechnology.

Plasmids, mutagenesis and shRNA

The Myc-SIRT1, Myc-SIRT6 and Myc-SIRT7 constructs were gifts from Dr. Jiadong Wang (54). Myc-SIRT1 was used to make GST-SIRT1 using the pGEX6T-1 vector (GE Healthcare). FLAG-RBMX, FLAG-PRPF3, FLAG-CDC5L, and FLAG-RBM25 were from Sino Biological. H2A cDNA and H2A-ub fusion constructs were constructed in the NBLV0051 vector (Novo Bio) using conventional molecular cloning methods.

PCR-based site-directed mutagenesis was performed according to standard procedures to create the H2A mutants. All clones were sequenced to confirm the presence of the desired mutations.

Silencing of endogenous CtIP by short hairpin RNAs (shRNAs) and small interfering RNAs (siRNAs) was performed as previously described (55,56). All the shRNA target sequences have been published and are listed as follows: ZRANB3, GAGUUACCUUAU-UGUGAAA; HLTF, GGAAUAUAAUGUUAACGAU; SMARCAL1, GCAGAAGAUCUACGACCUA; RAD51, CUAAUCAGGUGGUAGCUCA (57); CtIP, GAGCA-GACCUUUCUCAGUAUA; FANCM, GAACAA-GAUUCCUCAUUACUU; BRCA1, CAACAUGCC-CACAGAUCAACU; BRCA2, GAAGAAUGCAGGU-UUAAUA (58); SIRT1, GTTGGATGATATGACACTG (59); BMI1, UUAGCAUCUAGAAAGCUGUAAUGGC (60); and FANCD2, GGUCAGAGCUGUAUUAUUC (61).

Acid extraction of histones

Acid extraction of histones was carried out according to a previously published procedure (62). Briefly, cells were scraped and harvested into a clean 1.5-ml Eppendorf tube after being washed with phosphate buffered saline (PBS). All of the following steps were performed at 4°C. The samples were incubated for 1 h with lysis buffer (10mM Tris-HCl pH 8.0, 1 mM KCl, 1.5 mM MgCl$_2$, 1 mM DTT) containing protein inhibitors, then centrifuged at 10 000 *g* for 15 min. The supernatant was discarded, and the pellet was re-suspended in 0.4 N H$_2$SO$_4$ and incubated on a rotator overnight. Samples were then centrifuged at 16 000 *g* for 10 min. The supernatant was transferred to a fresh tube and trichloroacetic acid (TCA) was added drop by drop (to a final concentration of 33%). After incubation for 30 min, histones were pelleted by spinning at 16 000 *g* for 10 min. The histone pellet was washed with ice-cold acetone and air-dried at room temperature for 20 min. Next, the histone pellet was dissolved in an appropriate volume of water and subjected to western blot analysis with the indicated antibodies.

Protein purification and *in vitro* de-crotonylation assay

GST–SIRT1 was expressed in BL21 (DE3) cells and affinity-purified with glutathione-Sepharose 4B, according to the manufacturer's instructions (GE Healthcare). For the *in vitro* de-crotonylation assay, histone substrate purified from SIRT1-KO cells was mixed with recombinant SIRT1 enzyme at 37°C for 4 h in reaction buffer (50 mM Tris, pH 8.0, 137 mM NaCl, 2.7 mM KCl, 3mM NAD$^+$/[Zn^{2+}], 1

mM MgCl$_2$ and 1 mM DTT). The assay mixture was then analyzed by western blotting using the indicated antibodies.

DNA fiber analysis

DNA fiber analyses were performed as previously described (63). Briefly, cells were treated for 4 h with 0.5 mM hydroxyurea, pulse-labeled with CldU, then pulse-labeled with IdU in fresh medium. After trypsinization, cells were washed and resuspended in PBS. Then, 2 μl of cell suspension was placed on a glass slide, which was angled to allow DNA to spread, and lysed using lysis buffer. DNA was denatured with HCl and blocked with 5% bovine serum albumin (BSA) in PBS for 1 h after washing. Slides were stained with antibodies and sealed with coverslips. Slides were imaged using an Olympus IX81 FL microscope and analyzed using ImageJ software. At least 200 replication forks were analyzed per experimental condition, while the analysis shows the mean of three independent experiments. A track length of 1 μm measured in ImageJ corresponds to 2.59 kb (64).

In situ proximity ligation assay (PLA)

The *in situ* PLA was performed using Duolink PLA technology (Sigma-Aldrich), according to the manufacturer's instructions. Briefly, cells were treated with or without 2 mM hydroxyurea for 2 h then washed with PBS. Cells were then fixed in 2% formaldehyde in PBS (w/v) and permeabilized with 0.5% Triton X-100. Coverslips were blocked for 30 min and incubated with the respective primary antibodies overnight at 4°C. Then, anti-mouse PLUS and anti-rabbit MINUS PLA probes were coupled to the primary antibodies. After washing in buffer A (0.01 M Tris, 0.15 M NaCl and 0.05% Tween-20), PLA probes were ligated for 45 min at 37°C then washed. Coverslips were washed in buffer B (0.2 M Tris and 0.1 M NaCl) following amplification. Finally, the coverslips were mounted using Vectashield mounting media (Vector Laboratories) containing 4′,6-diamidino-2-phenylindole (DAPI), sealed, and imaged using an Olympus IX81 FL microscope.

iPOND

Isolation of proteins on nascent DNA (iPOND) experiments were carried out as previously described (65). Briefly, cells labeled with EdU were treated with 2 mM hydroxyurea for 2 h. Then, the cells were fixed with 1% formaldehyde in PBS, and the formaldehyde was quenched with 1.25 M glycine before the cells were harvested. Cells were then permeabilized with 0.25% Triton X-100 in PBS and incubated with click reaction buffer (biotin azide, 10 μM; sodium ascorbate, 10 mM, CuSO$_4$, 2 mM) for 80 min. Following the click reaction, the cells were sonicated in lysis buffer (1% [wt/vol] SDS in 50 mM Tris [pH 8.0]) and centrifuged at 13 000 rpm for 12 min. The lysates were incubated with streptavidin beads overnight at 4°C in the dark. Following this incubation, the beads were washed once with ice-cold lysis buffer, once with 1M NaCl, and twice more with ice-cold lysis buffer. Then, the beads were heated at 95°C in 2 × Laemmli buffer (4% SDS, 20% glycerol, 125 mM Tris

[pH 6.8], 0.1% [w/v] bromophenol blue and 0.25 M dithio-threitol [DTT]) for 20 min, loaded onto SDS-PAGE gels, then immunoblotted with the indicated antibodies.

Immunofluorescence

Immunofluorescence analyses were performed as previously described (66,67). Briefly, the cells were cultured on cover-slips at a concentration of 2×10^5 cells/well in a 6-well plate. After culture for 24 h, the coverslips were transferred to a 24-well plate, and the cells were washed with PBS. Following the removal of PBS, the cells were fixed in 1 ml of 100% ice-cold methanol at $-20°$C for 7 min, then blocked with 2% BSA solution in PBS containing 0.1% Tween-20 at 4°C overnight. Cells were then incubated with the appropriate antibodies at 4°C overnight. After washing three times with blocking buffer, the cells were incubated with appropriate secondary antibodies for 1 h at 37°C in the dark, then incubated in DAPI solution for 2 min. Cells were subjected to immunofluorescence analyses using an Olympus IX-81 fluorescence microscope.

RT-qPCR

Total RNA was extracted from the cell lines using TRIzol reagent (Invitrogen), following the manufacturer's instructions. Complementary DNA (cDNA) was synthesized by reverse transcription using a Hiscript cDNA synthesis kit (Vazyme). SYBR qPCR mix (Vazyme) was used to perform RT-qPCR on a Bio-Rad IQ5 real-time PCR system. The RT-qPCR assays used previously published primers (44) for specific genes: PFTK1F 5′ TGCAGAGGACCTGGC-CTCCA, PFTK1R 5′ TCCCAAAGGCCCGCATGCTT, METF 5′ GCCAACCGAGAGACAAGCATCTTCA, MET1R 5′ TGCTCCACCACTGGCAAAGC, RBM39F 5′ AGCAGTGCCAACGGCCATGA, RBM39R 5′ CTTCTTGAGCGGCTCCGTCGC, GAPDHF 5′ CCTGCCTCTACTGGCGCTGC, and GAPDHR 5′ CCTTGAGGGGGCCCTCCGAC.

Cell viability assay

Cells were seeded in 96-well plates (5000 cells/well), treated with different concentrations of hydroxyurea and doxoru-bicin for 72 h, then MTS (Promega, G3582) was added, and the mixture was incubated for 2 h. Cell viability was determined by measuring the emission at 490 nm on a Spectra-max M5 reader (Molecular Devices).

Chromatin immunoprecipitation (ChIP) assay

ChIP assays were carried out as previously described (58,68). Briefly, the cells were cross-linked with 1% formaldehyde for 10 min at room temperature, and the reaction was stopped with 125 mM glycine solution. After washing twice with cold PBS, the cells were resuspended in lysis buffer (1% SDS, 10 mM EDTA, 50 mM Tris-HCl, pH 8.1) supplemented with a protease inhibitor cocktail, then sonicated. Following sonication (Diagenode Bioruptor), the supernatants were collected by centrifugation, pre-cleared with Protein A/G Sepharose beads (Amersham

Biosciences) and subjected to immunoprecipitation with an RNA Pol II antibody (Abcam ab817). The pellet was washed sequentially with TSE I (0.1% SDS, 1% Triton X-100, 2 mM EDTA, 20 mM Tris-HCl, pH 8.1, 150 mM NaCl), TSE II (0.1% SDS, 1% Triton X-100, 2 mM EDTA, 20 mM Tris-HCl, pH 8.1, 500 mM NaCl), buffer III (0.25 M LiCl, 1% NP-40, 1% deoxycholate, 1 mM EDTA, 10 mM Tris-HCl, pH 8.1), and TE. Then, the protein–DNA complex was eluted from the beads with elution buffer (1% SDS, 0.1 M NaHCO$_3$), and cross-linking was reversed by adding 4 μl of 5 M NaCl and incubating at 65°C for 4 h. Proteins were digested with Proteinase K at 42°C for 2 h. DNA was extracted using a QIAquick kit (QIAGEN) according to the manufacturer's instructions. Recovered DNA was analyzed by RT-PCR using previously published ChIP primers (44): PFTK1F 5′ TAGTGCTCGCCCTTTCGC, PFTK1R 5′ ATC-CAAGCCTGTGCGCAAAA, METF 5′ TCCCTCGC-CTCAGGGGTTCTG, MET1R 5′ GCGCCCCTCTCC-CTCCTAAGT, RBM39F 5′ CTGCCTCCCACAAACT-GAAG, RBM39R 5′ CTACCTGGGGTGGGTAAT-GAG,WNT2F 5′ TTCACACCAACCTTCAGGGTA, WNT2R 5′ TGGATTCGGATGGTGGGAAC.GAPDHF 5′ GAAGCTGAGTCATGGGTAGT, and GAPDHR 5′ CCCGGTGACTTTACAGCCT.

Comet assay

Comet assays were carried out as previously described (69). Briefly, 10^5 cells were suspended in PBS, mixed with 1% of low-melting-point agarose, pipetted on to a slide precoated with 1% agarose, then covered with 0.5% low-melting-point agarose. The cells were lysed with lysis solution (2.5 M NaCl, 0.1 M EDTA, 10 mM Tris, 10% DMSO, 1% Triton-X100 [pH 10]) at 4°C for 2 h. Excess ions were washed off with double-distilled water, the slides were placed in a hor-izontal electrophoresis tank containing electrophoresis so-lution (1 mM Na$_2$EDTA, 300 mM NaOH [pH 13]) to soak for 20 min, and electrophoresis was run for 40 min. Fol-lowing electrophoresis, the slides were rinsed with neutral-ization buffer (0.4 M Tris, pH 7.5) for 15 min. The slides were then washed in distilled water for 5 min, stained with propidium iodide (PI, 5 μg/ml) for 20 min, and then excess PI was washed off with distilled water. The slides were ob-served under 590 nm excitation light using an Olympus IX-81 fluorescence microscope. At least 100 comet images from each slide were analyzed using comet image analysis soft-ware. Tail moment (TM) reflects both the tail length (TL) and the fraction of DNA in the comet tail (TM = %DNA in tail × TL/100).

Chromatin fractionation and immunoprecipitation

Chromatin fractionation was performed as previously de-scribed (67). Briefly, cells were washed with cold PBS and suspended in buffer A (10 mM HEPES [pH 7.0], 100 mM NaCl, 300 mM sucrose, 3 mM MgCl$_2$, protease inhibitor cocktail [Roche; EDTA-free], and 0.7% Triton X-100). Af-ter incubation on ice for 20 min, the lysate was centrifuged at 1500 g for 4 min at 4°C. The supernatant was designated S2. The nuclei were washed once with buffer A and then

lysed in 200 μl of buffer B (3 mM EDTA, 0.2 mm EGTA, 1 mM dithiothreitol, and protease inhibitor mixture). After a 10 min incubation on ice, soluble nuclear proteins (S3) were separated from chromatin by centrifugation (2000g, 5 min). Isolated chromatin (P4) was washed once with buffer B and centrifuged at high speed (13 000 *g*, 10 min). Then, the chromatin fraction was subjected to immunoprecipitation with M2 beads following a standard protocol.

S9.6-immunoprecipitation (S9.6-IP)

S9.6-IP was performed as previously described, with some modifications (70). Briefly, U2OS cells were lysed in lysis buffer (85 mM KCl, 5 mM PIPES [pH 8.0], 0.5% NP-40 and protease inhibitor cocktail) for 10 min on ice. Pelleted nuclei were re-suspended in IP buffer (10 mM Tris-HCl [pH 7.5], 200 mM NaCl, 2.5 mM MgCl$_2$, 0.1% SDS) and sonicated for 10 min. Extracts were treated with or without 5 U RNase H1 then subjected to IP with S9.6 antibody or immunoglobulin G (IgG) and protein G beads. After incubation at 4°C for 4 h, the beads were washed three times with IP buffer, re-suspended in IP buffer, treated with RNase A at 4°C for another 4 h, washed three times with IP buffer and eluted for the western blot analysis.

Statistical analysis

Data analyses were performed using GraphPad Prism 9 and Microsoft Excel software, as applicable. Significant differences were determined using an unpaired Student's *t*-test (RT-qPCR, ChIP, and cell viability assays) or a Mann–Whitney U test (PLA, DNA fiber analysis and other experiments). In all cases: n s., $P > 0.05$; *$P < 0.05$; **$P < 0.01$; ***$P < 0.001$; ****$P < 0.0001$.

RESULTS

H2AK119cr and H2AK119ub are reversibly modulated by replication stress

Previous MS data indicated the presence of Kcr at H2AK119 (H2AK119cr), but the biological function of this modification remains unclear (71). We speculated whether H2AK119cr is involved in the DDR and interacts with the ubiquitination of H2A on the same lysine residue. A commercial antibody against H2AK119cr (PTM-543, PTM Biolab) is available for the detection of H2AK119cr. We performed a dot-spot assay to further verify the specificity of this antibody with histone H2A or H3 derivatives, which had been chemically modified by crotonyl or acetyl. The results showed that the PTM-543 antibody recognized crotonylated H2A peptide (K119cr) but not unmodified H2A peptide (H2A), acetylated H2A peptides (K119ac and K118ac) or crotonylated H3 peptides (H3K9cr and H3K27cr). All crotonylated peptides were recognized by a pan anti-Kcr antibody (PTM-502, PTM Biolab), which was used to detect Kcr signals from all core histone proteins in a previous study (71), but only crotonylated H2A peptide (K119cr) was recognized by the PTM-543 antibody (Supplementary Figure S1A). Therefore, we used the PTM-543 antibody to detect K119cr in our subsequent experiments.

Histone Kcr was shown to be significantly enhanced when cells were cultured in a medium containing crotonate (71). Consistent with this finding, we found that the H2AK119cr signal increased after cells were cultured with crotonate (Figure 1A). The upregulation of H2AK119cr was accompanied by the downregulation of H2AK119ub in cells treated with crotonate, suggesting that H2AK119cr and H2AK119ub exist simultaneously in the cell and may influence each other. We wondered whether the switching from H2AK119cr to H2AK119ub is regulated by DNA damage and contributes to the DDR.

We checked the effect of various DNA damage-inducing agents on the global levels of H2AK119cr and H2AK119ub. Intriguingly, the topoisomerase I inhibitor camptothecin (Figure 1B) and the topoisomerase II inhibitors doxorubicin (Figure 1C) and etoposide (Supplementary Figure S1B) decreased global levels of H2AK119cr and increased H2AK119ub in the three indicated cell lines. Topoisomerase inhibitor treatment could induce both replication stress and replication-associated DSBs. The effects of these drugs on H2AK119cr and H2AK119ub could therefore be caused by either replication stress per se or replication stress-induced DSBs. Short-term hydroxyurea or low-concentration aphidicolin treatment, which cause replication fork stalling but do not induce high levels of DSBs, also decreased H2AK119cr and increased H2AK119ub (Figure 1D and E). The induction of H2AK119cr/H2AK119ub switching by replication stress occurred in the primary cell line MCF-10F (Figure 1F). Furthermore, the induction of H2AK119cr by replication stress was dependent on the hydroxyurea concentration (Supplementary Figure S1C) and required the presence of ATR kinase but not ATM kinase (Supplementary Figure S1D). Together, these results suggest that replication stress can reversibly modulate global levels of H2AK119cr and H2AK119ub.

SIRT1 mediates decrotonylation of H2AK119

As mentioned earlier, crotonyl groups on proteins can be enzymatically removed by HDACs. We next attempted to identify which HDACs are responsible for the decrotonylation of H2AK119 and so might be involved in the regulation of H2AK119cr during replication stress. Nicotinamide inhibits the NAD$^+$ (nicotinamide adenine dinucleotide)-dependent sirtuin family of HDACs (SIRT1 to SIRT7) (72), whereas trichostatin A inhibits class I and class II HDACs (73,74). Nicotinamide treatment but not trichostatin A treatment impaired hydroxyurea-induced downregulation of H2AK119cr (Figure 2A and B), suggesting that the sirtuin family of HDACs (but not class I and class II HDACs) mediate decrotonylation of H2AK119 during replication stress. Among the sirtuin family of proteins, SIRT1, SIRT6 and SIRT7 are primarily localized in the nucleus and regulate the DDR (75–80). Over-expression of SIRT1 but not SIRT6 or SIRT7 significantly reduced the level of H2AK119cr (Figure 2C). H2AK119cr was significantly increased (Figure 2D and Supplementary Figure S2B) in two SIRT1-KO cell lines constructed using CRISPR–Cas9 technology (Supplementary Figure S2A). These data suggest that SIRT1-mediated decrotonylation of H2AK119 occurs *in vivo*. To confirm this finding, an
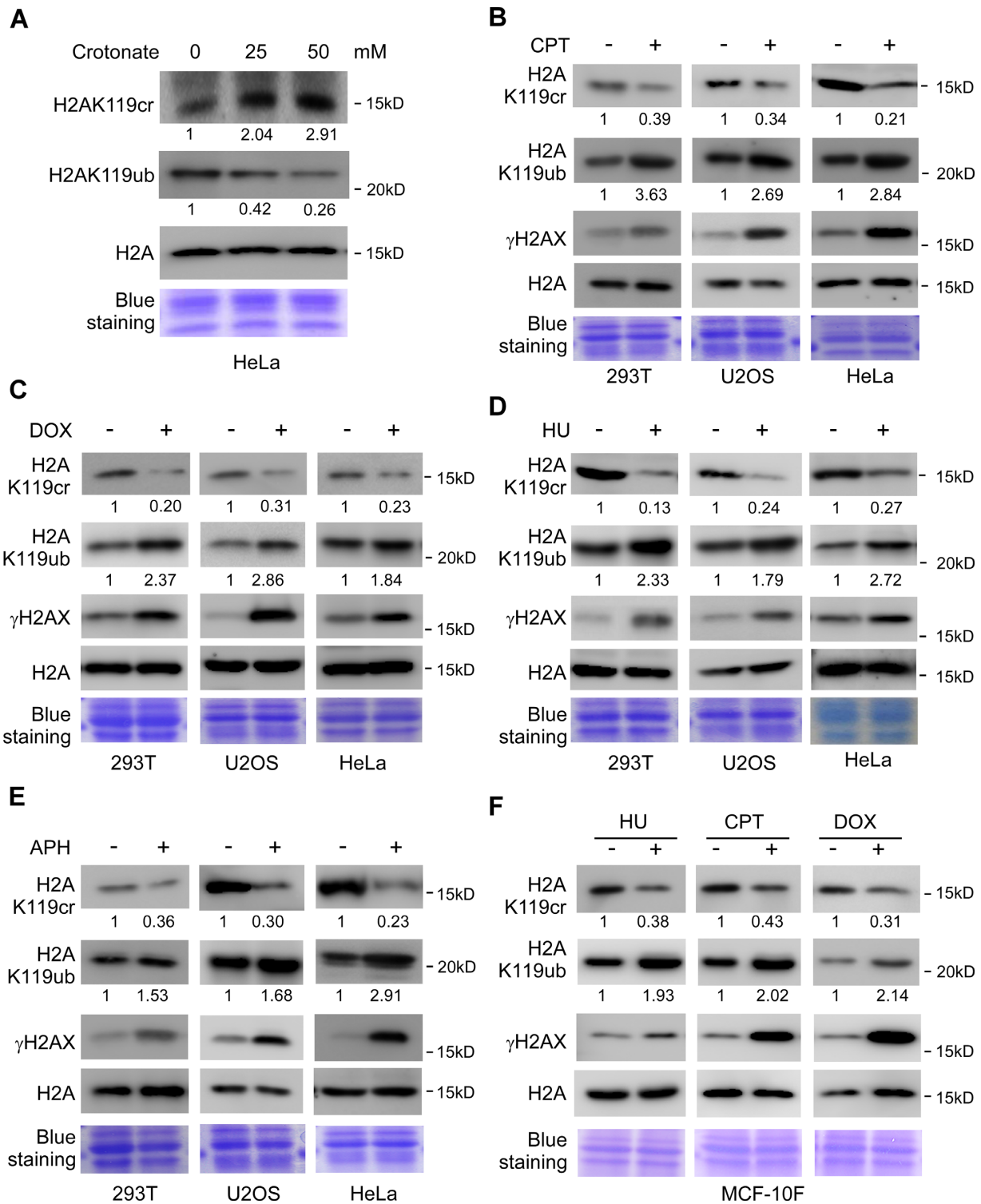
Figure 1.   Regulation of H2AK119cr and H2AK119ub by DNA damage. (**A**) Crotonate treatment increased the level of H2AK119cr but decreased the level of H2AK119ub. The histone proteins extracted from HeLa cells incubated with 0, 25 or 50 mM crotonate for 24 h were subjected to western blotting with the indicated antibodies. The blue staining shows the loading control. (**B**–**F**) After induction of DNA damage by the indicated method, histones from the indicated cells were prepared by acidic extraction and subjected to western blot analysis. γH2AX was used as a marker of DNA damage induction. The blue staining in the bottom panel shows the loading control. The methods used to induce DNA damage were camptothecin (CPT, 1 μM for 4 h), doxorubicin (DOX, 1.5 μM for 24 h), hydroxyurea (HU, 1 mM for 4 h) and aphidicolin (APH, 0.6 μM for 24 h). H2AK119cr and H2AK119ub blots were quantified using ImageJ software, and the normalized data are shown at the bottom of the blot.
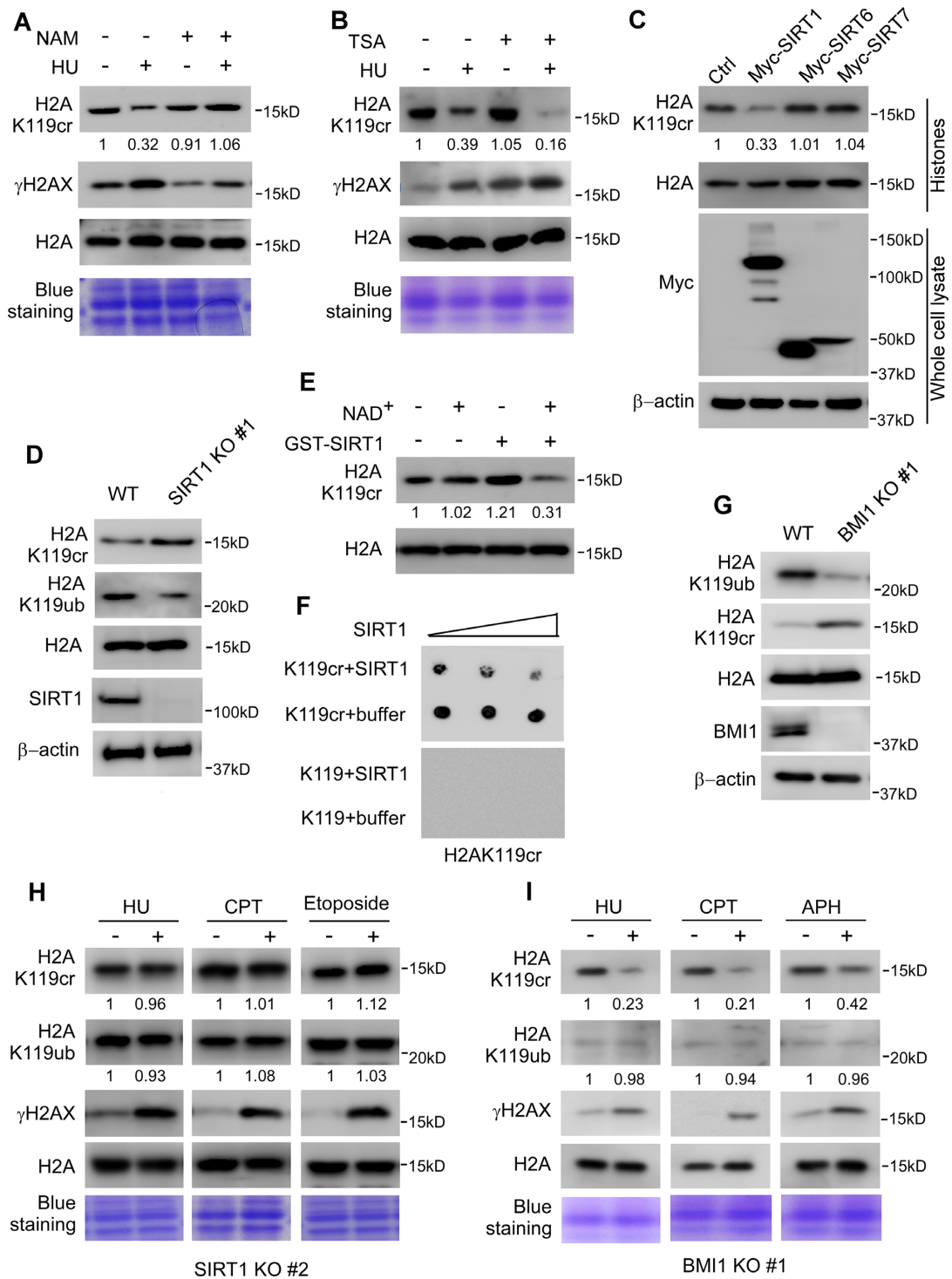
Figure 2. SIRT1 promotes decrotonylation and subsequent ubiquitination of H2AK119 during replication stress. (**A** and **B**) 293T cells were incubated with or without nicotinamide (NAM, 10 mM for 24 h, A) or trichostatin A (TSA, 1 μM for 24 h, B) then treated with 1 mM hydroxyurea for 4 h. After drug treatment, histones were extracted and subjected to western blot analysis using the indicated antibodies. γH2AX was used as a marker of DNA damage induction. The blue staining in the bottom panel shows the loading control. (**C**) Whole-cell lysates and histones were prepared from 293T cells transfected with the indicated construct and immunoblotted with the indicated antibodies. (**D**) Histones from wild-type (WT) or SIRT1-KO cells were analyzed by immunoblotting with the indicated antibodies. (**E**) *In vitro* decrotonylation assay using extracted histones from SIRT1-KO cells and purified SIRT1 enzyme. The reaction products were analyzed by western blotting with the indicated antibodies. (**F**) *In vitro* decrotonylation assay with crotonylated H2A peptides (K119cr) or uncrotonylated H2A peptides (K119) and increasing amounts of SIRT1 or buffer control. The reaction products were spotted on a nitrocellulose membrane and immunoblotted with an H2AK119cr antibody. (**G**) Histones from WT and BMI1-KO cells were analyzed by immunoblotting with the indicated antibodies. (**H** and **I**) SIRT1-KO cells (H) and BMI1-KO (I) cells were pre-treated with the indicated drugs. After drug treatment, histones were extracted and subjected to western blot analysis using the indicated antibodies. H2AK119cr and H2AK119ub blots were quantified using ImageJ software, and the normalized data are shown at the bottom of the blot.

in vitro decrotonylation assay was performed using histones from SIRT1-KO cells or crotonylated H2A peptide (K119cr) and purified SIRT1 (Supplementary Figure S2C). The results showed that SIRT1 decrotonylated both purified H2A protein (Figure 2E) and crotonylated H2A peptide (Figure 2F) in the presence of NAD$^+$ *in vitro*. Furthermore, a SIRT1 deacetylase activity-deficient mutant, SIRT1 HY (H363Y) (81), was unable to remove the crotonylation of H2AK119 either *in vivo* (Supplementary Figure S2D) or *in vitro* (Supplementary Figure S2C, S2E). It is well established that BMI1, a component of the canonical polycomb repressive complex 1 (PRC1) (82,83), plays an important role in modifying H2AK119 by ubiquitin (47,82,84) and is involved in the DDR (85–87). Chromatin histones isolated from BMI1-KO cell lines generated using CRISPR–Cas9 technology (Supplementary Figure S2F) decreased H2AK119ub levels and increased H2AK119cr levels (Figure 2G and Supplementary Figure S2G). This result further supports the notion that H2AK119cr and H2AK119ub might influence each other in the cellular environment. H2AK119cr was not downregulated by hydroxyurea, camptothecin or etoposide treatment in SIRT1-KO cells (Figure 2H). Intriguingly, however, levels of H2AK119ub also did not change after treatment with hydroxyurea, camptothecin or etoposide (Figure 2H), indicating that decrotonylation of H2AK119 by SIRT1 is a prerequisite for subsequent ubiquitination at this site during replication stress. In BMI1-KO cells, replication stress induced by hydroxyurea, camptothecin or aphidicolin no longer promoted H2AK119ub (Figure 2I), suggesting that BMI1 is also responsible for H2AK119ub during replication stress. However, hydroxyurea, camptothecin and aphidicolin treatment still significantly reduced H2AK119cr levels in BMI1-KO cells (Figure 2I), suggesting that replication stress-induced decrotonylation of H2AK119 is not affected by BMI1 or BMI1-mediated H2AK119ub.

H2AK119ub/H2AK119cr accumulates at reversed replication forks

H2AK119ub concentrates locally at sites of UV radiation-induced lesions and DSBs (48–53). In response to mild replication stress, remodeling of stalled forks can generate a reversed, four-way Holliday junction-like structure by annealing the two nascent strands behind the stalled fork and re-annealing the parental strands (88–90). The annealed nascent strands form a 3′ overhang containing single-end DSBs (Figure 3A), which can serve as a platform to recruit multiple DDR factors (91). We next wondered whether H2AK119ub/H2AK119cr also accumulates at reversed replication forks and helps cells alleviate replication stress.

We first used the iPOND technique (92,93) to examine H2AK119ub signals at stalled replication forks. Consistent with previously reported findings, we observed γH2AX (93), which marks DSBs, at stalled replication forks in hydroxyurea-treated 293T and HCT116 cells (Figure 3B and C). Hydroxyurea treatment also significantly increased H2AK119ub in the two cell lines (Figure 3B and C). The data indicated that H2AK119ub accumu-

lated at stalled replication forks. We performed *in situ* PLAs to confirm this finding. As previously reported (94), we detected a strong nuclear PLA signal using antibodies against CtIP and RPA2 in hydroxyurea-treated U2OS cells (Supplementary Figure S3A), indicating that stalled and reversed replication forks formed in these cells. Under the same experimental conditions, we observed the formation of hydroxyurea-induced H2AK119ub/RPA2 PLA foci (Supplementary Figure S3B); this finding was consistent with the iPOND result. Strikingly, we did not find obvious H2AK119ub/RPA2 PLA foci in SIRT1-KO or BMI1-KO cells (Supplementary Figure S3B), indicating that SIRT1-mediated decrotonylation and BMI1-mediated ubiquitination are required for H2AK119ub to accumulate at the hydroxyurea-arrested replication fork. We next labeled cells with the thymidine analog EdU (5-ethynyl-29-deoxyuridine), then performed a PLA using antibodies against H2AK119ub and EdU (93,95). As shown in Figure 3D, hydroxyurea treatment increased the number of H2AK119ub/EdU PLA foci in U2OS cells (Figure 3D) and MCF-10F primary cells (Supplementary Figure S3C). H2AK119ub/EdU PLA foci were not present in SIRT1-KO and BMI1-KO U2OS cells (Figure 3D) or MCF-10F cells in which SIRT1 or BMI1 was depleted by shRNA (Supplementary Figure S3C). These data confirm that H2AK119ub associates with nascent DNA during replication stress. We did not observe obvious hydroxyurea-induced H2AK119cr/EdU PLA foci in wild-type cells (Figure 3E). However, we found significant H2AK119cr/EdU PLA foci in SIRT1-KO cells in the presence of hydroxyurea (Figure 3E). These findings support the notion that H2AK119cr accumulates at stalled replication forks in the absence of SIRT1. In wild-type cells, SIRT1 removes crotonylation from H2AK119 under replication stress, thus allowing other modifications, such as ubiquitination, to take place at the same lysine residues.

The recombinase RAD51 and several translocases, including HLTF, ZRANB3, SMARCAL1 and FANCM, are required for replication fork reversal (88–90,96–99). Depletion of each translocase or Rad51 dramatically reduced hydroxyurea-induced H2AK119ub/EdU PLA foci and H2AK119ub/RPA2 PLA foci in wild-type cells (Figure 3F; Supplementary Figure S3D and Figure S3E). Depletion of each translocase also significantly reduced H2AK119cr/EdU PLA foci in SIRT1-KO cells (Figure 3G). These data suggest that replication fork reversal is important for H2AK119ub/H2AK119cr accumulation. Once a Holliday junction is formed, several DSB repair factors, such as BRCA1, BRCA2 and CtIP, protect nascent DNA strands against degradation by nucleases and stabilize the reversed replication fork (94,100,101). Depletion of BRCA1, BRCA2 or CtIP significantly reduced hydroxyurea-induced H2AK119ub/RPA2 PLA foci (Figure 3H and Supplementary Figure S3E) and H2AK119ub/EdU PLA foci (Figure 3I and Supplementary Figure S3E). These results indicate that stabilized Holliday junctions are required for the accumulation of H2AK119ub at the stalled replication fork. Together, these findings suggest that H2AK119ub/H2AK119cr accumulate at reversed stalled replication forks during replication stress.
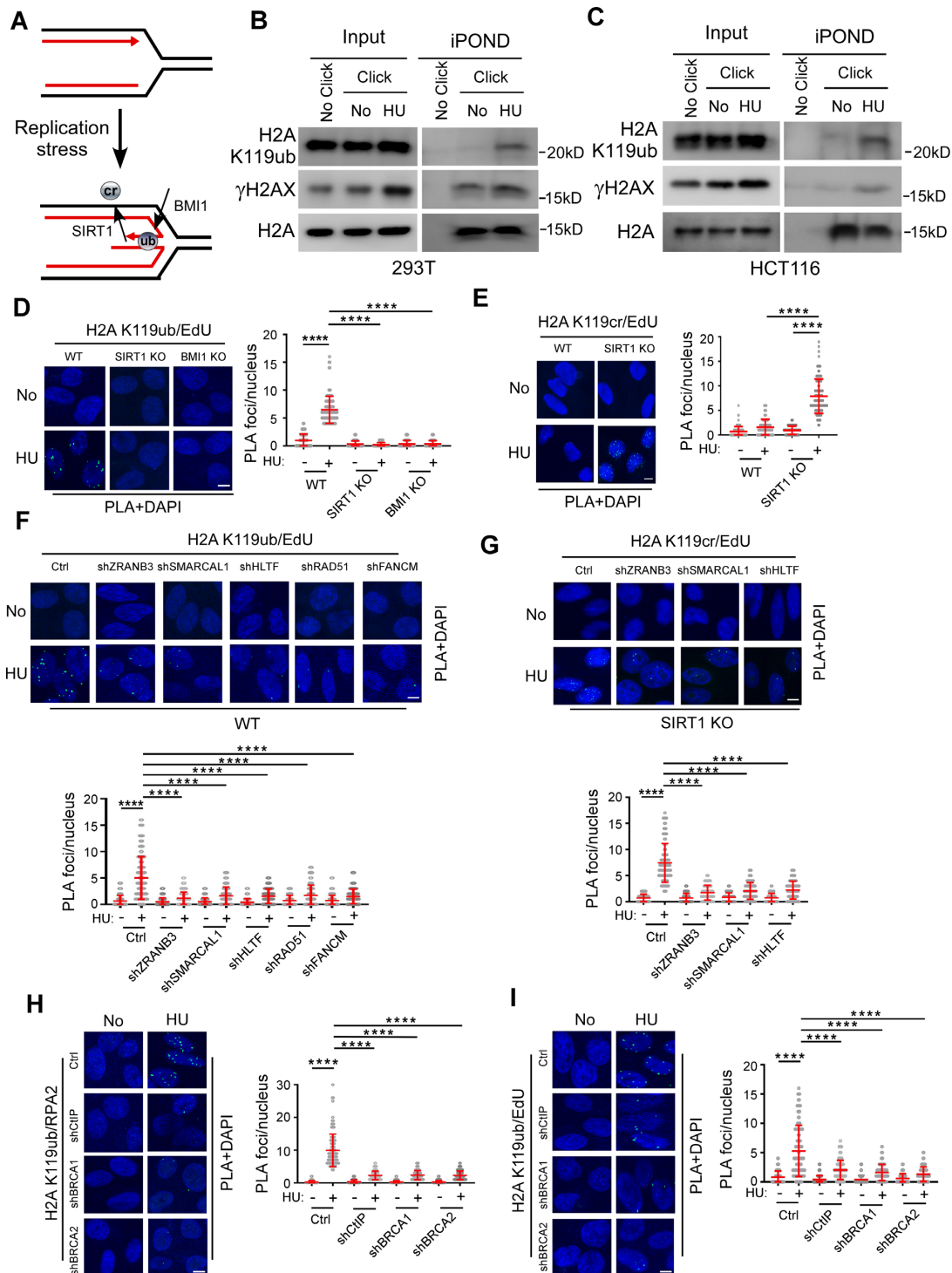
Figure 3. H2AK119ub/H2AK119cr accumulates at reversed replication forks. (**A**) A model showing the accumulation of H2AK119ub/H2AK119cr at a reversed replication fork. (**B** and **C**) 293T cells (B) and HCT116 cells (C) were labeled with EdU for 10 min prior to the addition of 2 mM hydroxyurea. Following the iPOND procedure, the input and iPOND samples were subjected to western blot analysis with the indicated antibodies. In no-click samples (no click), biotin azide was replaced by DMSO. (**D**) The H2AK119ub-nascent DNA (EdU) interaction was analyzed by PLA in U2OS cells (WT) treated with or without (no) 2 mM hydroxyurea for 4 h. Left, representative images. Right, quantification of the average number of PLA foci per nucleus. (**E**) The H2AK119cr-nascent DNA (EdU) interaction was analyzed by PLA in SIRT1-KO cells treated with or without (no) 2 mM hydroxyurea for 4 h. Left, representative images. Right, quantification of the average number of PLA foci per nucleus. (**F** and **G**) U2OS cells (WT) or SIRT1-KO cells were infected with lentiviruses encoding the indicated shRNAs or a control vector (ctrl), The H2AK119ub- EdU (F) and H2AK119cr-EdU (G) interactions were analyzed by PLA using the method described in panels (D and E). (**H** and **I**) U2OS cells (WT) and SIRT1-KO cells were infected with lentiviruses encoding the indicated shRNAs or a control vector (ctrl). The H2AK119ub- RPA2 (H) and H2AK119ub-EdU interactions (I) were analyzed by PLA using the method described in panels (D and E). In panels (D–I), scale bar = 10 μm. Data represent means ± SD from three independent experiments; ****$P < 0.0001$, Mann–Whitney test.

SIRT1 and BMI1 operate in the same pathway to coordinate transcription and replication in response to replication stress

We analyzed DNA fiber spreading to test the effect of SIRT1 and BMI1 on the progression of individual replication forks during replication stress. As shown in Figure 4A, depletion of SIRT1 or BMI1 decreased the replication speed during replication stress. As reported previously, acute depletion of BMI1 by RNA interference (RNAi) technology increases the level of TRCs in unperturbed cells (102,103). We next asked whether SIRT1 and BMI1 reduce TRCs to facilitate DNA replication during replication stress. As revealed by PLA foci formation, SIRT1 and BMI1 were recruited to hydroxyurea-induced stalled replication forks (Figure 4B and Supplementary Figure S4A). Meanwhile, hydroxyurea (Figure 4C) and doxorubicin (Supplementary Figure S4B) also induced the formation of Pol II/PCNA PLA foci, suggesting the formation of TRCs. SIRT1-KO U2OS cells and BMI1-KO U2OS cells contained more Pol II/PCNA PLA foci than wild-type (WT) cells in the presence of hydroxyurea (Figure 4C) or doxorubicin (Supplementary Figure S4B). MCF-10F primary cells expressing SIRT1 or BMI1 shRNA also contained more Pol II/PCNA PLA foci than cells expressing shRNA control in the presence of hydroxyurea (Supplementary Figure S4C), suggesting that SIRT1 and BMI1 play important roles in preventing TRCs during replication stress. Moreover, knockdown of BMI1 in SIRT1-KO cells or knockdown of SIRT1 in BMI1-KO cells (Supplementary Figure S4D) did not further increase the levels of hydroxyurea- (Figure 4C) or doxorubicin-induced (Supplementary Figure S4B) Pol II/PCNA PLA foci. Knockdown of FANCD2 in SIRT1-KO cells and BMI1-KO cells further enhanced the levels of hydroxyurea-Pol II/PCNA PLA foci (Figure 4C and Supplementary Figure S4D). These data suggest that BMI1 and SIRT1 operate in the same pathway but both work in different pathways with FANCD2 to suppress replication stress-induced TRCs. As mentioned earlier, TRCs are generally associated with R-loop formation. Therefore, we used immunostaining with an S9.6 antibody to examine R-loop formation (104) to further confirm our finding. As expected, we observed an increase in R-loop formation after hydroxyurea (Figure 4D) or doxorubicin (Figure 4E) treatment in wild-type cells. Depletion of either SIRT1 or BMI1 further increased hydroxyurea- (Figure 4D) and doxorubicin-induced (Figure 4E) R-loop levels. Consistent with what we observed in the Pol II/PCNA PLA foci analysis, knockdown of BMI1 in SIRT1-KO cells or SIRT1 in BMI1-KO cells did not further increase hydroxyurea- or doxorubicin-induced R-loop levels (Figure 4D and E). Furthermore, we observed significantly increased interactions between R-loops (S9.6 antibody) and H2AK119ub in wild-type cells following hydroxyurea treatment by the PLA (Supplementary Figure S4E) and S9.6-IP (Supplementary Figure S4F) experiments, with the interaction between R-loops and H2AK119ub clearly destroyed by RNase H1, indicating that an association between R-loops and H2AK119ub did occur under replication stress. We thus concluded that SIRT1 and BMI1 operate in the same pathway to coordinate transcription and replication during replication stress.

SIRT1 and BMI1 regulate the transcription of genes near stalled replication forks

In response to hydroxyurea and doxorubicin treatment, ATR kinase promotes the degradation of the histone chaperone ASF1a (anti-silencing function protein 1 homologue a), which leads to histone eviction, RNA Pol II release, and transcription repression specifically in the vicinity of stalled forks (44). These effects may help cells to reduce TRCs and avoid genome instability (35). Surprisingly, we found that doxorubicin-induced ASF1a degradation did not occur in all the cell lines we tested. Doxorubicin-induced ASF1a degradation occurred in, for example, U2OS cells and HeLa cells. In other cell lines, such as HCT116 cells and 293T cells, doxorubicin treatment did not change the expression level of ASF1a (Supplementary Figure S5), suggesting mechanisms additional to or instead of the ATR-ASF1a axis are involved in resolving TRCs in these cells. We thus wondered whether SIRT1-mediated H2AK119cr removal and BMI1-mediated H2AK119ub can resolve TRCs that cause transcription repression in the vicinity of stalled replication forks. We used RT-qPCR technology to examine the mRNA levels of three genes that are regulated by hydroxyurea and doxorubicin (44), before and after treatment with hydroxyurea or doxorubicin. Consistent with previous findings (44), the mRNA levels of the three selected genes, which were located near the stalled replication forks, were downregulated by doxorubicin in U2OS, 293T, and HCT116 cells (Figure 5A–C). However, doxorubicin treatment did not alter the mRNA levels of these genes in SIRT1-KO cells (Figure 5D) or BMI1-KO cells (Figure 5E). Intriguingly, doxorubicin treatment reduced the enrichment of H2AK119cr but increased the enrichment of H2AK119ub in these genes (Figure 5F and G). The effects of ASF1a degradation on TRCs occur mainly by reducing the loading of RNA Pol II on newly replicated DNA (44). The results of our RNA Pol II ChIP assays confirmed that doxorubicin reduced RNA Pol II loading and further showed that doxorubicin treatment did not alter the enrichment of RNA Pol II on three selected genes in SIRT1-KO cells and BMI1-KO cells (Figure 5H). These data indicate that SIRT1 and BMI1 suppress the transcription of genes located near stalled replication forks by displacing RNA Pol II to ameliorate replication stress-induced TRCs. H2AK119cr/H2AK119ub switching, which is mediated by SIRT1 and BMI1, may play a role in this process.

Depletion of SIRT1 and BMI1 increases replication stress-induced DSBs

Thus far, we have shown that SIRT1-mediated H2AK119cr removal and BMI1-mediated H2AK119ub are associated with replication stress-induced TRCs. We next wondered whether these processes can reduce the chromosome breakage and associated genome instability that are the major consequence of TRCs. Using immunofluorescence staining (IF), we observed hydroxyurea- (Figure 6A) and doxorubicin-induced (Figure 6B) γH2AX foci in wild-type cells; these foci mark the DSB damage site. In the presence of hydroxyurea (Figure 6A) or doxorubicin (Figure 6B), more γH2AX foci were formed in SIRT1-KO cells and
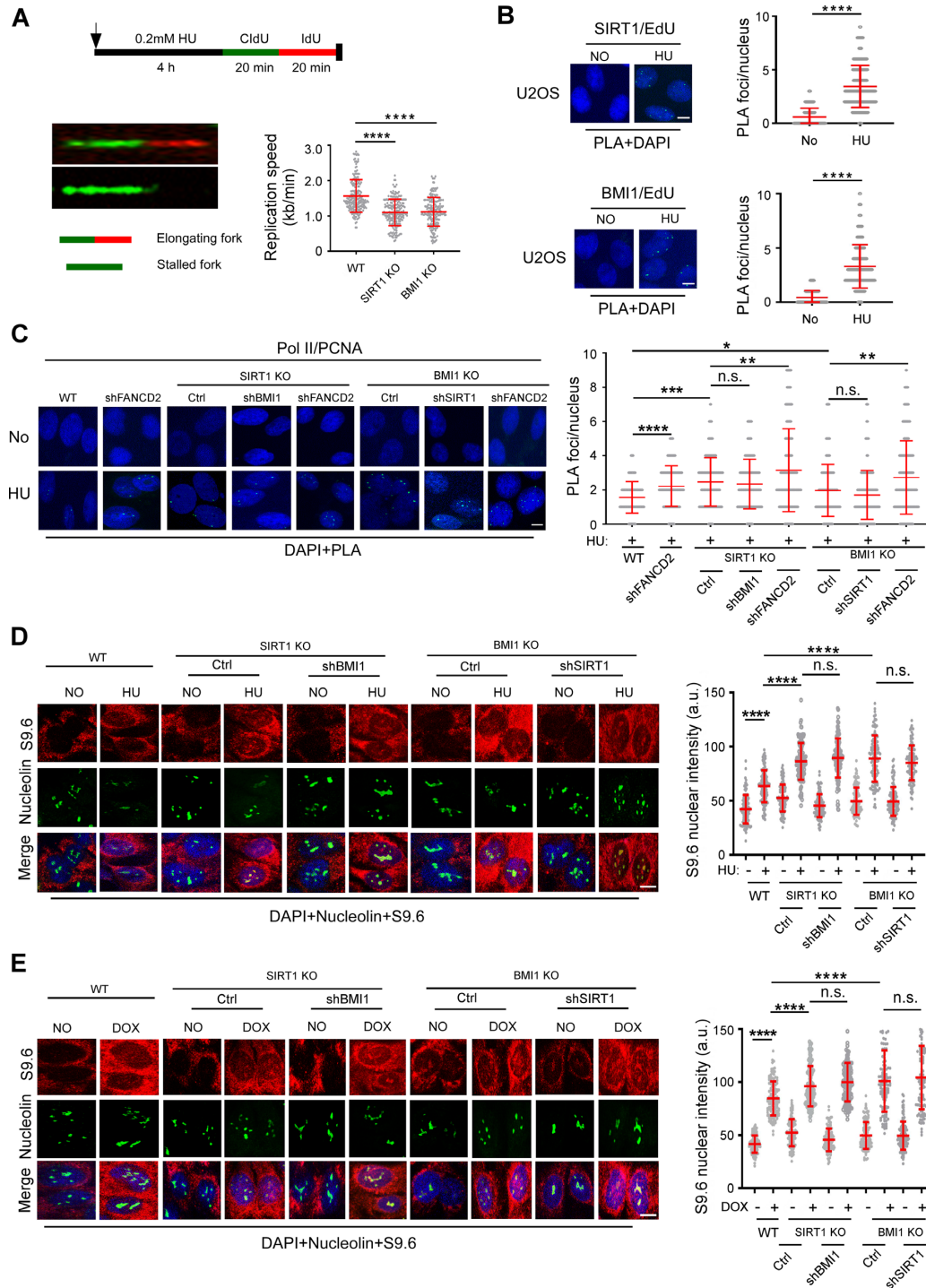
Figure 4. Depletion of SIRT1 or BMI1 during replication stress increases TRCs. (**A**) Depletion of SIRT1 or BMI1 increases replication stress. (Top) (A) Schematic showing how replication speed was measured using DNA fiber analysis. U2OS cells were pre-treated with 0.2 mM hydroxyurea for 4 h then sequentially pulse-labeled with CldU (green) and IdU (red) for 20 min each in the presence of hydroxyurea. Representative DNA fibers show an elongating fork and a stalled fork (bottom, left). The length of the IdU (red) fibers in the elongating fork was measured using ImageJ software and used to calculate the speed of the replication fork. The scatterplot shows the quantification of the speed of replication fork from at least 200 fibers (bottom right). (**B**) Recruitment of SIRT1 (top) and BMI1 (bottom) to stalled forks was analyzed by PLA assays. U2OS cells were treated with or without (no) 2 mM hydroxyurea for 4 h; then, SIRT1/EdU PLA assays and BMI1/EdU PLA assays were performed as previously described. Left, representative images. Right, quantification of the average number of PLA foci per nucleus. (**C**) Parental (WT), SIRT1-KO, and BMI1-KO U2OS cells expressing vector control (ctrl) or the indicated shRNA were treated with 0.5 mM hydroxyurea for 12 h, then PLA between PCNA and RNA pol II was performed. Left, representative images of PLA foci (green). Right, the scatterplot shows the quantification of the PLA signal per nucleus from at least 100 cells. (**D** and **E**) The cells used and treated as described in panel (C) were subjected to immunostaining. Left, representative immunostaining images. Right, quantification of S9.6 nuclear signal intensity following nucleolar signal removal. In all panels, data are plotted from three independent experiments with means ± SD. The P-values are indicated as $*P < 0.05$, $**P < 0.01$, $***P < 0.001$, $****P < 0.0001$., n.s., not significant; Mann–Whitney test; scale bar, 10 μm.
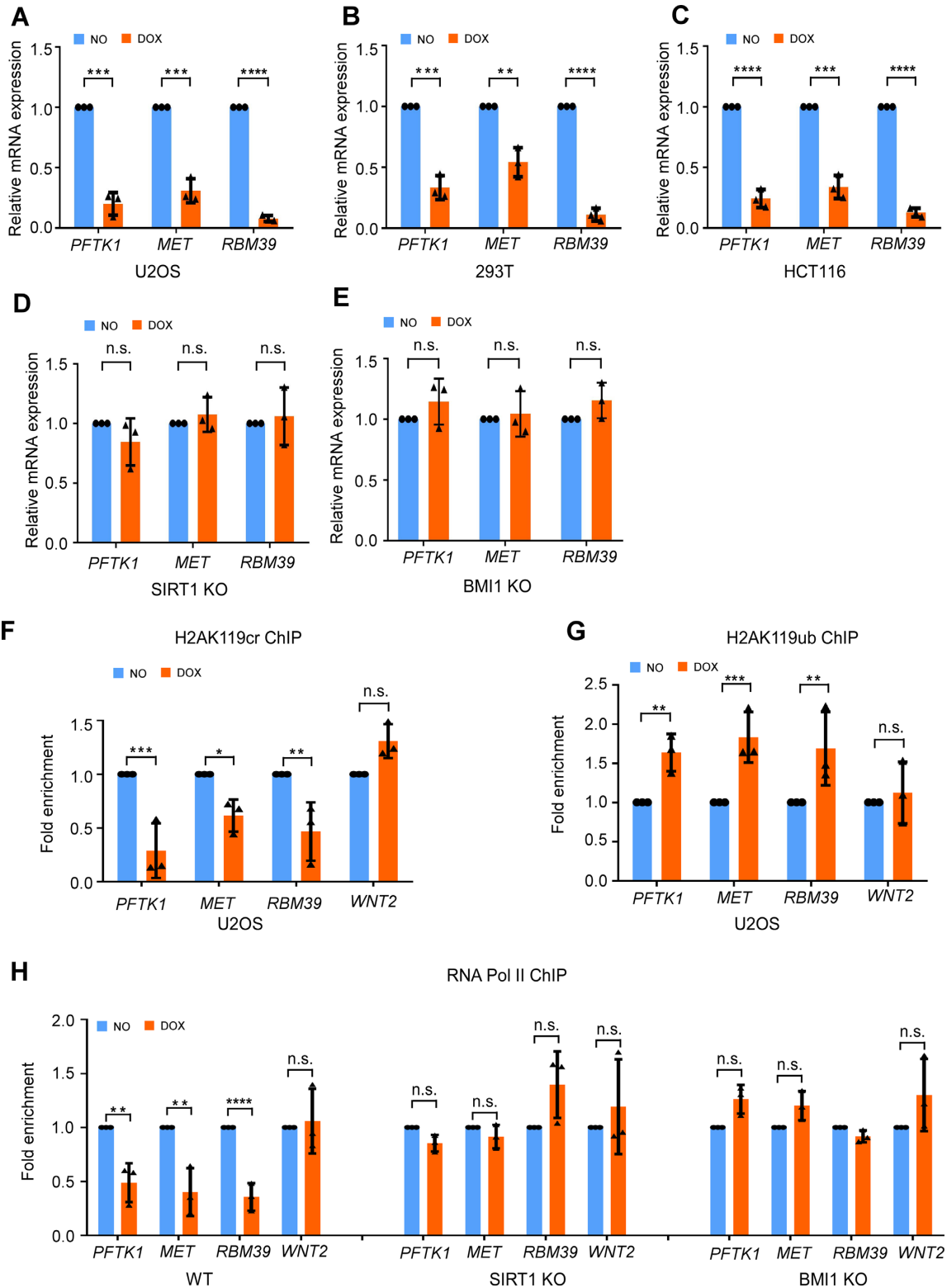
Figure 5. SIRT1 and BMI1 are required for the transcriptional repression of genes near the stalled replication fork. (**A**–**E**) Relative mRNA levels of the indicated genes were examined by RT-qPCR in U2OS (A), 293T (B), HCT116 (C), SIRT1-KO (D) and BMI1-KO (E) cells treated with DMSO or doxorubicin. (**F** and **G**) H2AK119cr (F) and H2AK119ub (G) ChIP assays of selected genes were performed in U2OS cells treated with DMSO or doxorubicin. The ChIP value in the DMSO-treated cells was set as 1 for normalization. (**H**) RNA Pol II ChIP assays of the selected genes were performed in U2OS cells, SIRT1-KO, and BMI1-KO cells treated with DMSO or doxorubicin. The ChIP value in the DMSO-treated cells was set as 1 for normalization. In all panels, data represent the means ± SD of three independent experiments. The *P*-value is indicated as *$P < 0.05$, **$P < 0.01$, ***$P < 0.001$, ****$P < 0.0001$., n.s., not significant; Student's *t*-test.
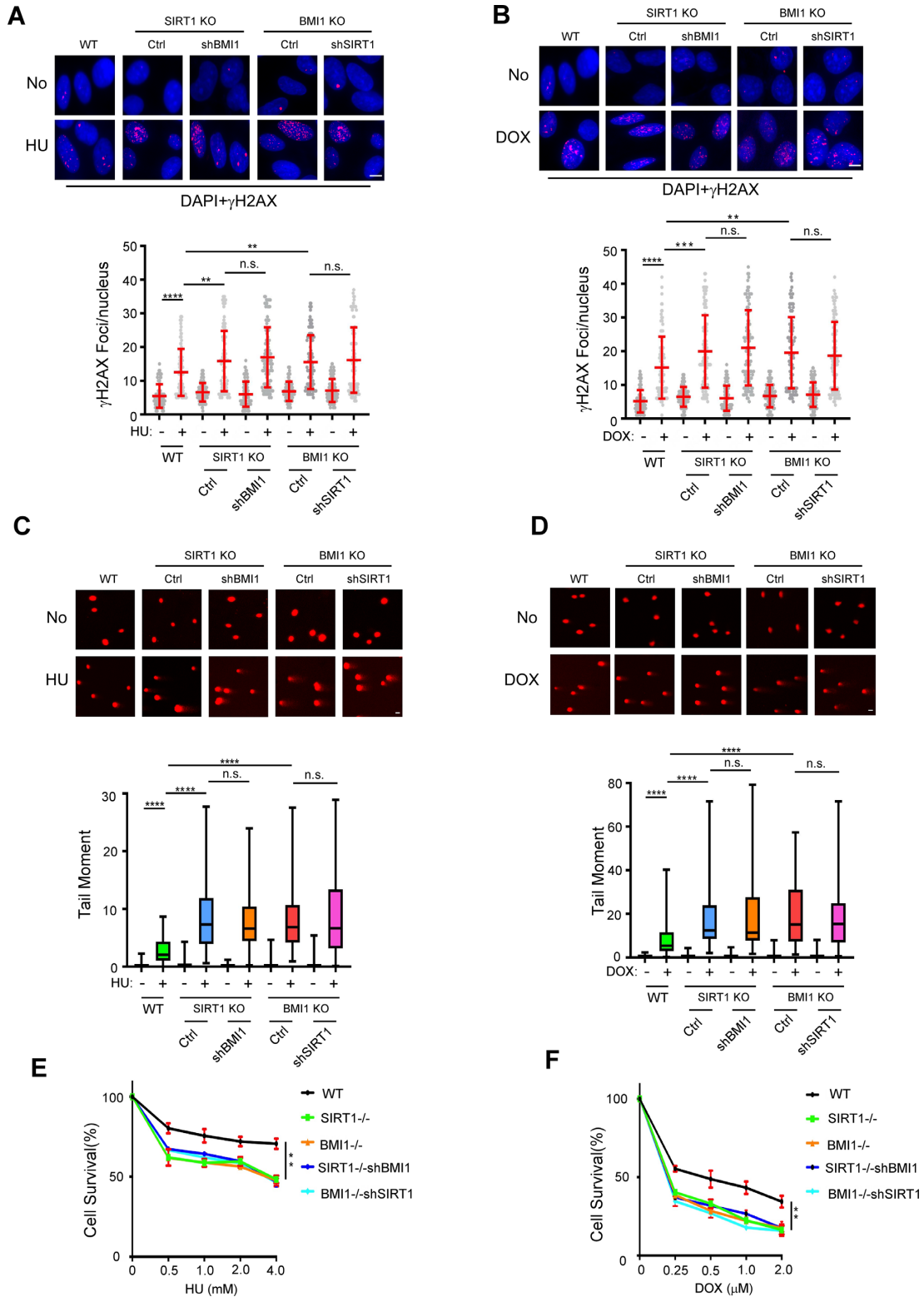
Figure 6. BMI1 and SIRT1 prevent replication stress-induced DNA breaks. (**A** and **B**) Parental (wild-type, WT), SIRT1-KO, and BMI1-KO U2OS cells expressing vector control (ctrl) or the indicated shRNA were treated with 1 mM hydroxyurea for 4 h (A) or 0.5 μM doxorubicin for 12 h; (B) then, immunostaining using a γH2AX antibody was performed. Representative immunostaining images are shown; scale bar: 10 μm. The scatterplot shows quantification of the number of γH2AX foci per nucleus from at least 100 cells. (**C** and **D**) The cells used and treated as described in panels (A and B) were subjected to an alkaline comet assay. Representative images are shown; scale bar: 40 μm. The scatterplot shows quantification of the tail moment in the indicated cell. (**E** and **F**) The cells used as described in panels (A and B) were treated with the indicated concentrations of hydroxyurea (E) or doxorubicin (F) for 72 h, then a cell viability assay was performed. In panels (A–D), the *P*-values were calculated using the Mann–Whitney test. In panels (E and F), the *P*-values were calculated using the Student's *t*-test.The *P*-values are indicated as **P < 0.01, ***P < 0.001, ****P < 0.0001, n.s., not significant.

BMI1-KO cells than in wild-type cells, suggesting there were more DSBs in SIRT1-KO cells and BMI1-KO cells. Knockdown of BMI1 in SIRT1-KO cells or SIRT1 in BMI1-KO cells did not further increase γH2AX foci formation (Figure 6A and B), suggesting SIRT1 and BMI1 operate in the same pathway to prevent the generation of DSBs. We confirmed the IF result by alkaline single-cell electrophoresis (comet assay). The depletion of either SIRT1 or BMI1 alone significantly increased comet tail formation in the presence of hydroxyurea (Figure 6C) or doxorubicin (Figure 6D), while co-depletion of SIRT1 and BMI1 did not result in further DNA injury (Figure 6C and D). Furthermore, SIRT1-KO cells and BMI1-KO cells were more sensitive to the effects of hydroxyurea (Figure 6E) or doxorubicin (Figure 6F) than wild-type cells, but co-depletion of SIRT1 and BMI1 did not increase the sensitivity of cells to hydroxyurea (Figure 6E) or doxorubicin (Figure 6F). Together, these data demonstrate that SIRT1 and BMI1 play important roles in preventing DNA breakage caused by replication stress. This finding is consistent with the functions of SIRT1 and BMI1 in resolving TRCs.

H2AK119cr/H2AK119ub switching is involved in resolving replication stress-induced TRCs

We generated stable cell lines bearing exogenous wild-type H2A (WT) or mutant H2AK119R using a lentivirus system, to test whether H2AK119cr and H2AK119ub are directly involved in resolving TRCs. Subnuclear fractionation of these cells showed that both wild-type H2A and mutant H2AK119R can be incorporated into cellular chromatin (Figure 7A). K119cr occurred in the wild-type H2A but not in the K119R mutant and was significantly down-regulated after treatment with hydroxyurea (Figure 7B), suggesting that it can occur on exogenously expressed H2A and be induced by replication stress. Cells expressing the mutant H2AK119R showed a significant increase in hydroxyurea-induced Pol II/PCNA PLA foci (Figure 7C) and R-loop formation (Figure 7D), suggesting that H2AK119cr/H2AK119ub is important for the coordination of replication and transcription under replication stress and to reduce TRCs.

SIRT1 regulates cell function by deacylating many substrates. To demonstrate that SIRT1 can indeed resolve TRCs by targeting H2AK119, we need to test whether H2A or its variants can restore the function of SIRT1 in resolving TRCs. However, in the absence of SIRT1, the wild-type H2A or any H2A variant in which K119 is mutated loses the H2AK119cr/H2AK119ub switching ability, thus H2AK119ub cannot be formed and the function of SIRT1 in resolving TRCs cannot be restored. It has previously been reported that artificial ubiquitin-H2A (H2Aub) fusion proteins can be incorporated into cellular chromatin and mimic the function of natural ubiquitin-histone H2A (105,106). We generated H2A2KR and H2A2KR-ub fusion proteins (Figure 7E), in which lysine residues at sites 118 and 119 were mutated to arginine residues, so that the fusion protein could be used to explore its function in the absence of BMI1-mediated endogenous ubiquitination modifications. In addition, all seven lysine residues on ubiqui-

tin were mutated to prevent chain formation. SIRT1-KO cells were transduced with lentivirus expressing H2A2KR or H2A2KR-ub fusion protein (Figure 7E). Compared with H2A2KR, expression of the H2A2KR-ub fusion protein significantly reduced hydroxyurea- and doxorubicin-induced Pol II/PCNA PLA foci (Figure 7F and Supplementary Figure S6A) and R-loop formation (Figure 7G and Figure S6B) in SIRT1-KO cells. These data suggest that the H2A-2KRub fusion protein rescues defects in the resolution of TRCs in SIRT1-KO cells. During replication stress, SIRT1 mainly targets H2AK119 to resolve TRCs.

DISCUSSION

Although lysine acetylation (Kac) has been widely studied, the detailed biological functions of lysine crotonylation (Kcr) modification remain largely unknown. In the present study, we found that crotonylation of H2AK119 antagonizes mono-ubiquitination on the same lysine residue during replication stress. We showed that H2AK119cr and H2AK119ub exist simultaneously in the cell. During replication stress, SIRT1 promotes decrotonylation of H2AK119. Removal of a crotonyl group from H2AK119 allows other modifications, such as ubiquitination, to occur. Replication stress can increase the speed of switching from H2AK119cr to H2AK119ub. However, this finding does not necessarily mean that the switching cannot occur in unperturbed cells. Indeed, we observed decreased H2AK119ub in SIRT1-KO cells and increased H2AK119cr in BMI1-KO cells (Figure 2D, G; Supplementary Figure S2B and Figure S2G). These data suggest that the switching may occur in unperturbed cells without the need for stimulation by replication stress. We thus speculate that antagonism of H2AK119cr to H2AK119ub is needed for unperturbed cells to maintain H2AK119ub within a certain range. Without H2AK119cr, H2AK119ub may accumulate at more chromosomal regions, which may cause unnecessary transcriptional suppression.

Currently, we still do not know what the abundance of H2AK119cr is in cells. It may not be as abundant as H2AK119ub, but only occurs in regions prone to forming clusters of stalled replication forks under replication stress, such as near the dormant origin (107). H2AK119cr can thus accumulate locally to compete with H2AK119ub. Our data showed that hydroxyurea-induced H2AK119cr/EdU PLA foci can form in SIRT1-KO cells (Figure 3E), suggesting that H2AK119cr can accumulate at hydroxyurea-arrested replication forks in the absence of SIRT1. As the global levels of H2AK119cr did not increase following hydroxyurea treatment under the same conditions (Figure 2H), we speculate that the local accumulation of H2AK119cr at stalled forks shown by the PLA results was not due to the recruitment of a crotonylase, which catalyzes crotonylation at the H2A K119 site, to stalled forks. In fact, SIRT1-KO cells contained more crotonylated H2A than wild-type cells (Figure 2D and Supplementary Figure S2B), and crotonylated H2A may be more easily recruited to the stalled fork in SIRT1-KO cells, resulting in local enrichment of H2AK119cr. It has been reported that the reverse replication fork undergoes re-chromatinization during replica-
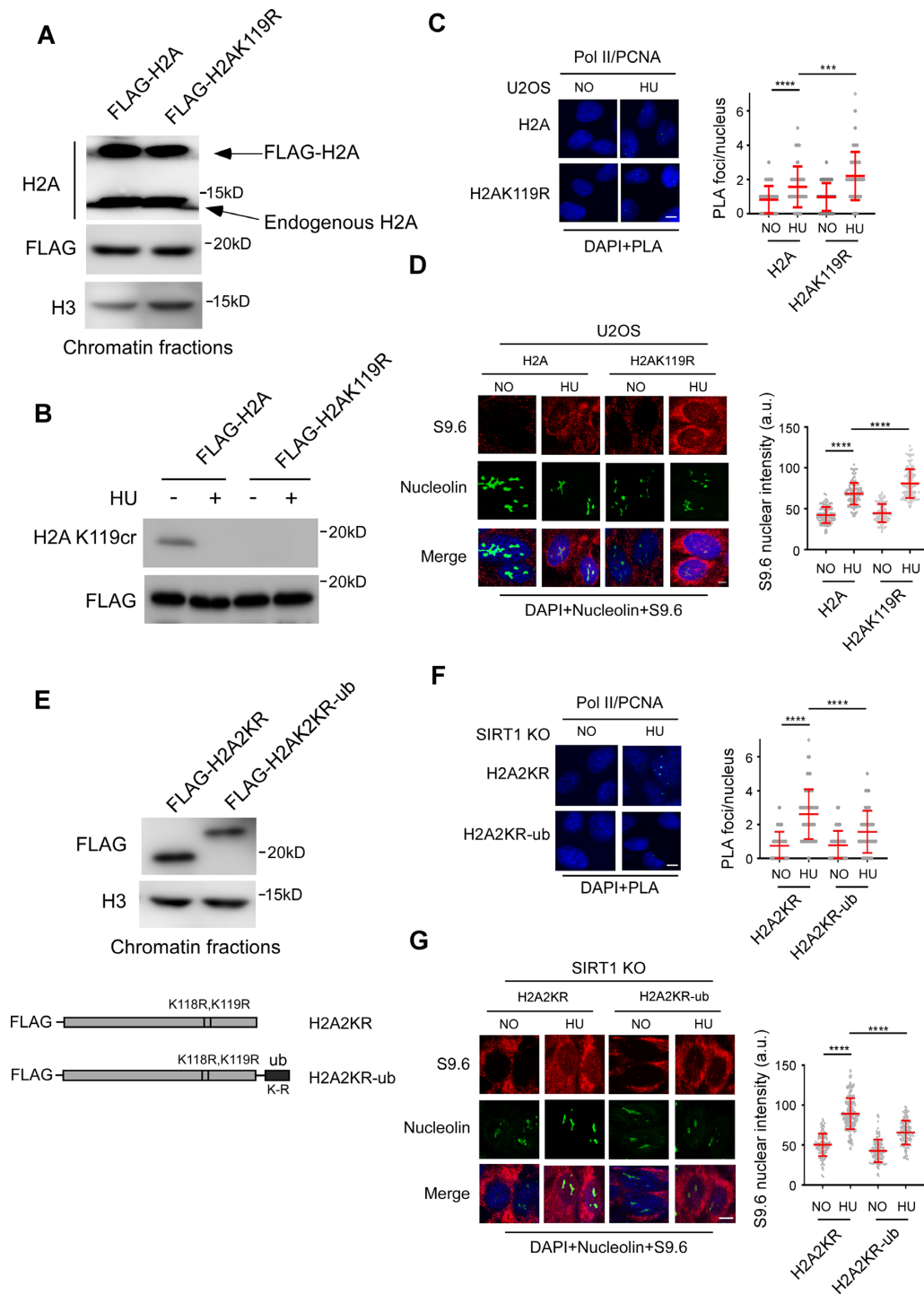
Figure 7. H2AK119cr and H2AK119ub are involved in resolving replication stress-induced TRCs. (**A**) Chromatin fractions were extracted from cells expressing FLAG-H2A or mutant FLAG-H2K119R and analyzed by western blot using the indicated antibodies. (**B**) Cells expressing FLAG-H2A or FLAG-H2K119R were treated with or without 1 mM hydroxyurea for 4 h. The chromatin fractions were extracted and subjected to immunoprecipitation with M2 beads followed by immunoblotting. (**C**) U2OS cells expressing FLAG-H2A or mutant FLAG-H2AK119R were treated with or without (no) 0.5 mM hydroxyurea for 12 h, then subjected to a PCNA/RNA Pol II PLA assay. Representative images of PLA foci and the quantification of PLA signals per nucleus are shown. (**D**) Cells used and treated as described in panel C were subjected to immunostaining using an S9.6 antibody. Representative images and the quantification of the S9.6 nuclear signal intensity following nucleolar signal removal are shown. (**E**) Top, chromatin fractions were extracted from SIRT1-KO cells expressing FLAG-H2A2KR or FLAG-H2A2KR-ub fusion constructs and analyzed by western blot. Bottom, a schematic representation of FLAG-H2A2KR and FLAG-H2K1192KR-ub fusion constructs. In both the H2A2KR and fusion constructs, H2A carried a lysine-to-arginine mutation at lysine 118 (K118) and lysine 119 (K119). In the fusion constructs, seven lysines in the ubiquitin were mutated to arginine. (**F and G**) SIRT1-KO cells expressing FLAG-H2A2KR or FLAG-H2A2KR fusion were subjected to a PCNA/RNA Pol II PLA assay (F), as described in panel C, or immunostaining (G), as described in panel D. In panels C, D, F and G, the data plotted are means ± SD from three independent experiments. The *P*-values are indicated as ***$P < 0.001$, ****$P < 0.0001$. Mann–Whitney test; scale bar: 10 μm.

tion stress (107). We can therefore reasonably speculate that crotonylated H2A may be more easily incorporated into the nascent DNA at the stalled replication fork, which results in local H2AK119cr accumulation. H2AK119cr on stalled replication forks may play special roles or may be rapidly removed by SIRT1 to allow H2AK119ub to occur. In line with this notion, H2AK119cr is likely crucial for cell recovery from the replication stress response once the replication stress has been relieved. The presence of accumulated crotonyl groups at H2AK119 may reduce the likelihood of the residue being re-modified by ubiquitin and thus expedite the cell's recovery from the H2AK119ub-mediated response. Further in-depth studies are needed to address these interesting issues.

H2AK119ub is a well-known PTM associated with DSB damage. H2AK119ub is observed at ionizing radiation-induced foci (IRIF) and is involved in both DSB-induced signaling and local transcription silencing (48–51,53). In the current study, we revealed another function of this classical epigenetic marker induced by chromosomal structural change. We showed that H2AK119ub accumulated at stalled replication forks. Individual depletion of RAD51 or DNA translocases (ZRANB3, SMARCAL1, HLTF and FANCM) implicated in replication fork reversal (89,96–99,108) was sufficient to block the accumulation of H2AK119ub at the stalled replication fork (Figure 3F and S3D). These data support the notion that the reversal of replication forks is required for the recruitment of H2AK119ub. Furthermore, the loss of fork-protection factors such as BRCA1/2 and CtIP (90,94,100,109–111), which stabilize the regressed arm at the reversed fork by preventing over-resection of nascent DNA, also reduces the accumulation of H2AK119ub at stalled replication forks (Figure 3H and I). We thus propose that reversed replication forks with nascent DNA may attract H2AK119ub and associated DDR factors. The regressed arms at reversed replication forks are regularly achromatized and show normal nucleosomal organization (91), which allows H2AK119ub or other histone modifications to occur. Indeed, RNF168, a key ubiquitin ligase in the DDR, is attracted and activated locally by reversed replication forks in unperturbed cells. RNF168-initiated H2AK13/15ub causes the assembly of classical DDR factors on the reversed replication fork to promote the efficient restart of the stalled fork and help cells to overcome endogenous replication difficulties (91). Our work thus adds new evidence for this assembly pathway, involving alternative DDR factors. The accumulation of H2AK119ub at the DSB damage region is dependent on ATM kinase activity (53). However, our results suggest that decrotonylation of H2AK119 induced by replication stress relies on ATR but not ATM kinase (Supplementary Figure S1D). Thus, these two pathways may have different assembly and regulatory mechanisms. Identifying which DDR factors or related PTMs are involved in this ATR-dependent pathway and how they play a role in the DDR network will be an important line of investigation for future studies.

The treatment of human cells with hydroxyurea or doxorubicin preferentially induces clusters of stalled replication forks in regions where there are actively expressed genes. The stalled replication forks undergo histone eviction due to ATR checkpoints and ubiquitination/proteasome pathway-mediated degradation of the histone chaperone ASF1a. ASF1a removal leads to histone eviction, RNA Pol II release and transcription repression near the stalled transcription forks. These effects thus reduce TRCs induced by hydroxyurea or doxorubicin and protect the integrity of the genome (35,44). We showed that doxorubicin-induced ASF1a degradation did not occur in all of the cell lines tested (Supplementary Figure S5), suggesting that the ATR–ASF1a axis is not the only cellular mechanism that is activated in response to hydroxyurea- or doxorubicin-induced TRCs. Given that H2AK119ub is always associated with transcription inhibition, it is reasonable to speculate that H2AK119ub can resolve TRCs. We performed a series of experiments to test this possibility and showed that SIRT1/BMI1 epistasis suppresses TRCs and associated R-loop formation during hydroxyurea- and doxorubicin-induced replication stress. Replacing endogenous H2A with mutant H2AK119R, which does not undergo SIRT1-/BMI1-mediated H2AK119cr/H2AK119ub switching, significantly affected the release of TRCs induced by hydroxyurea (Figure 7C and D), suggesting that SIRT1/BMI1 could modulate replication stress-induced TRCs through H2AK119. H2AK2KRub fusion reconstituted the ability of SIRT1-KO cells to resolve TRCs, showing that H2AK119ub is a direct executor of TRC resolution. How does H2AK119cr/H2AK119ub achieve this? Our interpretation of the mechanism is shown in Figure 8. Co-directional transcription and replication are not the major sources of TRCs, which explains why low levels of TRCs and associated R-loops were detected in unperturbed cells (Figure 8, 1). However, hydroxyurea- or doxorubicin-induced replication stress will induce dormant origin firing in gene-rich parts of the genome, which reduces the proportion of replication forks co-oriented with transcription, thus increasing the likelihood of head-on collisions and associated R-loop formation (Figure 8, 2). Due to constant replication stress, the replication forks arising from dormant origin firing will stall, reverse, and recruit SIRT1 and BMI1 to remove H2AK119cr and accumulate H2AK119ub in the nascent DNA (Figure 8, 3). A chromosome that is modified by H2AK119ub may block RNA Pol II binding, thus causing the release of RNA Pol II, transcription repression, and reduced TRCs (Figure 8, 4). The data we present here show that SIRT1-/BMI1-mediated dynamic switching of H2AK119cr to H2AK119ub plays an important role in resolving TRCs induced by replication stress.

Sirt1 is the most studied sirtuin, it is able to remove both Kac and Kcr from histones and is involved in many biological processes, through multiple targets. One limitation of our work was the failure to distinguish whether SIRT1 is involved in resolving TRCs through deacetylation or decrotonylation activity. Previous pioneering work identified HDAC1 and HDAC3 mutants with impaired deacetylation but intact decrotonylation activity, which greatly promoted research into the function of Kcr (112). In the future, the identification of a mutant that can separate decrotonylation activity from deacetylation activity in SIRT1 would be very useful.
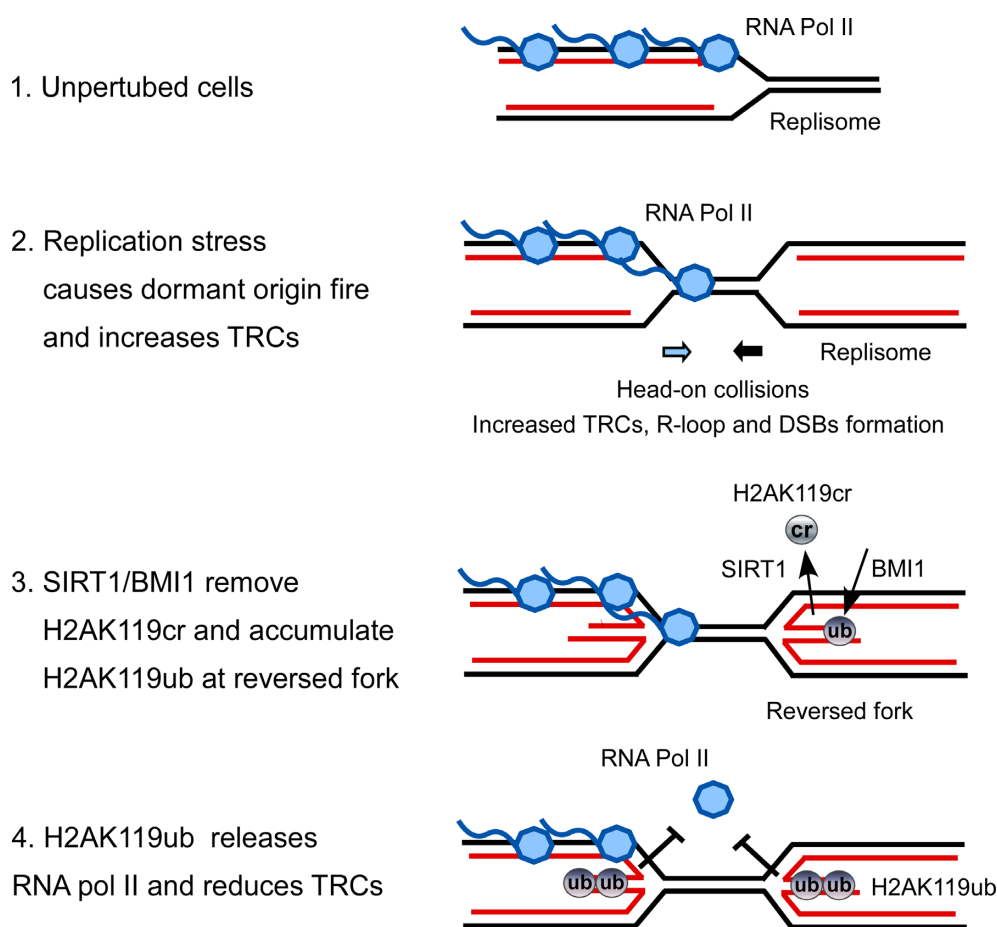
Figure 8. A proposed model for the role played by H2AK119cr and H2AK119ub in resolving replication stress-induced TRCs (see Discussion for more details).

DATA AVAILABILITY

All data generated and analyzed during this study are included in this published article and its supplementary data files.

SUPPLEMENTARY DATA

Supplementary Data are available at NAR Online.

ACKNOWLEDGEMENTS

FUNDING

REFERENCES

1. Ciccia,A. and Elledge,S.J. (2010) The DNA damage response: making it safe to play with knives. *Mol. Cell*, **40**, 179–204.
2. Jackson,S.P. and Bartek,J. (2009) The DNA-damage response in human biology and disease. *Nature*, **461**, 1071–1078.
3. Hoeijmakers,J.H.J. (2009) DNA damage, aging, and cancer. *New Engl. J. Med.*, **361**, 1914–1914.
4. Varon,R., Vissinga,C., Platzer,M., Cerosaletti,K.M., Chrzanowska,K.H., Saar,K., Beckmann,G., Seemanova,E., Cooper,P.R., Nowak,N.J. *et al.* (1998) Nibrin, a novel DNA double-strand break repair protein, is mutated in nijmegen breakage syndrome. *Cell*, **93**, 467–476.
5. Savitsky,K., Barshira,A., Gilad,S., Rotman,G., Ziv,Y., Vanagaite,L., Tagle,D.A., Smith,S., Uziel,T., Sfez,S. *et al.* (1995) A single ataxia-telangiectasia gene with a product similar to pi-3 kinase. *Science*, **268**, 1749–1753.
6. Wang,W.D. (2007) Emergence of a DNA-damage response network consisting of fanconi anaemia and BRCA proteins. *Nat. Rev. Genet.*, **8**, 735–748.
7. Sabari,B.R., Zhang,D., Allis,C.D. and Zhao,Y.M. (2017) Metabolic regulation of gene expression through histone acylations. *Nat. Rev. Mol. Cell Bio.*, **18**, 90–101.
8. Huang,H., Sabari,B.R., Garcia,B.A., Allis,C.D. and Zhao,Y.M. (2014) SnapShot: histone modifications. *Cell*, **159**, 458.
9. Chen,Y., Sprung,R., Tang,Y., Ball,H., Sangras,B., Kim,S.C., Falck,J.R., Peng,J.M., Gu,W. and Zhao,Y.M. (2007) Lysine propionylation and butyrylation are novel post-translational modifications in histones. *Mol. Cell Proteomics*, **6**, 812–819.
10. Dai,L.Z., Peng,C., Montellier,E., Lu,Z.K., Chen,Y., Ishii,H., Debernardi,A., Buchou,T., Rousseaux,S., Jin,F.L. *et al.* (2014)

Lysine 2-hydroxyisobutyrylation is a widely distributed active histone mark. *Nat. Chem. Biol.*, **10**, 365–U373.

11. Xie,Z.Y., Dai,J.B.A., Dai,L.Z., Tan,M.J., Cheng,Z.Y., Wu,Y.M., Boeke,J.D. and Zhao,Y.M. (2012) Lysine succinylation and lysine malonylation in histones. *Mol. Cell Proteomics*, **11**, 100–107.

12. Tan,M.J., Peng,C., Anderson,K.A., Chhoy,P., Xie,Z.Y., Dai,L.Z., Park,J., Chen,Y., Huang,H., Zhang,Y. *et al.* (2014) Lysine glutarylation is a protein posttranslational modification regulated by SIRT5. *Cell Metab*, **19**, 605–617.

13. Tan,M.J., Luo,H., Lee,S., Jin,F.L., Yang,J.S., Montellier,E., Buchou,T., Cheng,Z.Y., Rousseaux,S., Rajagopal,N. *et al.* (2011) Identification of 67 histone marks and histone lysine crotonylation as a new type of histone modification. *Cell*, **146**, 1015–1027.

14. Xie,Z.Y., Zhang,D., Chung,D.J., Tang,Z.Y., Huang,H., Dai,L.Z., Qi,S.K., Li,J.Y., Colak,G., Chen,Y. *et al.* (2016) Metabolic regulation of gene expression by histone lysine beta-Hydroxybutyrylation. *Mol. Cell*, **62**, 194–206.

15. Choudhary,C., Weinert,B.T., Nishida,Y., Verdin,E. and Mann,M. (2014) The growing landscape of lysine acetylation links metabolism and cell signalling. *Nat. Rev. Mol. Cell Bio.*, **15**, 536–550.

16. Sabari,B.R., Tang,Z.Y., Huang,H., Yong-Gonzalez,V., Molina,H., Kong,H.E., Dai,L.Z., Shimada,M., Cross,J.R., Zhao,Y.M. *et al.* (2015) Intracellular Crotonyl-CoA stimulates transcription through p300-Catalyzed histone crotonylation. *Mol. Cell*, **58**, 203–215.

17. Ntorla,A. and Burgoyne,J.R. (2021) The regulation and function of histone crotonylation. *Front. Cell Dev. Biol.*, **9**, 624914.

18. Wan,J.H., Liu,H.Y., Chu,J. and Zhang,H.Q. (2019) Functions and mechanisms of lysine crotonylation. *J. Cell Mol. Med.*, **23**, 7163–7169.

19. Baumann,K. (2015) Crotonylation versus acetylation. *Nat. Rev. Mol. Cell Bio.*, **16**, 265–265.

20. Liu,X.G., Wei,W., Liu,Y.T., Yang,X.L., Wu,J., Zhang,Y., Zhang,Q., Shi,T.L., Du,J.X., Zhao,Y.M. *et al.* (2017) MOF as an evolutionarily conserved histone crotonyltransferase and transcriptional activation by histone acetyltransferase-deficient and crotonyltransferase-competent CBP/p300. *Cell Discov.*, **3**, 17016.

21. Fellows,R., Denizot,J., Stellato,C., Cuomo,A., Jain,P., Stoyanova,E., Balazsi,S., Hajnady,Z., Liebert,A., Kazakevych,J. *et al.* (2018) Microbiota derived short chain fatty acids promote histone crotonylation in the colon through histone deacetylases. *Nat. Commun.*, **9**, 105.

22. Liu,S., Yu,H., Liu,Y., Liu,X., Zhang,Y., Bu,C., Yuan,S., Chen,Z., Xie,G., Li,W. *et al.* (2017) Chromodomain protein CDYL acts as a Crotonyl-CoA hydratase to regulate histone crotonylation and spermatogenesis. *Molecular Cell*, **67**, 853–866.

23. Yu,H., Bu,C., Liu,Y., Gong,T., Liu,X., Liu,S., Peng,X., Zhang,W., Peng,Y., Yang,J. *et al.* (2020) Global crotonylome reveals CDYL-regulated RPA1 crotonylation in homologous recombination-mediated DNA repair. *Sci. Adv.*, **6**, eaay4697.

24. Abu-Zhayia,E.R., Machour,F.E. and Ayoub,N. (2019) HDAC-dependent decrease in histone crotonylation during DNA damage. *J. Mol. Cell Biol.*, **11**, 804–806.

25. Dutta,D., Shatalin,K., Epshtein,V., Gottesman,M.E. and Nudler,E. (2011) Linking RNA polymerase backtracking to genome instability in e. coli.*Cell*, **146**, 533–543.

26. French,S. (1992) Consequences of replication fork movement through transcription units in vivo. *Science*, **258**, 1362–1365.

27. Liu,B. and Alberts,B.M. (1995) Head-on collision between a DNA replication apparatus and RNA polymerase transcription complex. *Science*, **267**, 1131–1137.

28. Merrikh,H., Machon,C., Grainger,W.H., Grossman,A.D. and Soultanas,P. (2011) Co-directional replication-transcription conflicts lead to replication restart. *Nature*, **470**, 554–557.

29. Sankar,T.S., Wastuwidyaningtyas,B.D., Dong,Y., Lewis,S.A. and Wang,J.D. (2016) The nature of mutations induced by replication-transcription collisions. *Nature*, **535**, 178–181.

30. Srivatsan,A., Tehranchi,A., MacAlpine,D.M. and Wang,J.D. (2010) Co-orientation of replication and transcription preserves genome integrity. *PLoS Genetics*, **6**, e1000810.

31. Hamperl,S., Bocek,M.J., Saldivar,J.C., Swigut,T. and Cimprich,K.A. (2017) Transcription-Replication conflict orientation modulates R-Loop levels and activates distinct DNA damage responses. *Cell*, **170**, 774–786.

32. Helmrich,A., Ballarino,M., Nudler,E. and Tora,L. (2013) Transcription-replication encounters, consequences and genomic instability. *Nat. Struct. Mol. Biol.*, **20**, 412–418.

33. Bowry,A., Kelly,R.D.W. and Petermann,E. (2021) Hypertranscription and replication stress in cancer. *Trends Cancer*, **7**, 863–877.

34. Hamperl,S. and Cimprich,K.A. (2016) Conflict resolution in the genome: how transcription and replication make it work. *Cell*, **167**, 1455–1467.

35. Garcia-Muse,T. and Aguilera,A. (2016) Transcription-replication conflicts: how they occur and how they are resolved. *Nat. Rev. Mol. Cell Bio.*, **17**, 553–563.

36. Lang,K.S., Hall,A.N., Merrikh,C.N., Ragheb,M., Tabakh,H., Pollock,A.J., Woodward,J.J., Dreifus,J.E. and Merrikh,H. (2017) Replication-Transcription conflicts generate R-Loops that orchestrate bacterial stress survival and pathogenesis. *Cell*, **170**, 787–799.

37. Boubakri,H., de Septenville,A.L., Viguera,E. and Michel,B. (2010) The helicases DinG, rep and UvrD cooperate to promote replication across transcription units in vivo. *EMBO J.*, **29**, 145–157.

38. Merrikh,C.N., Brewer,B.J. and Merrikh,H. (2015) The b. subtilis accessory helicase PcrA facilitates DNA replication through transcription units. *PLoS Genetics*, **11**, e1005289.

39. Million-Weaver,S., Samadpour,A.N., Moreno-Habel,D.A., Nugent,P., Brittnacher,M.J., Weiss,E., Hayden,H.S., Miller,S.I., Liachko,I. and Merrikh,H. (2015) An underlying mechanism for the increased mutagenesis of lagging-strand genes in bacillus subtilis. *Proc. Natl. Acad. Sci. USA*, **112**, E1096–E1105.

40. Million-Weaver,S., Samadpour,A.N. and Merrikh,H. (2015) Replication restart after replication-transcription conflicts requires RecA in bacillus subtilis. *J. Bacteriol.*, **197**, 2374–2382.

41. Paul,S., Million-Weaver,S., Chattopadhyay,S., Sokurenko,E. and Merrikh,H. (2013) Accelerated gene evolution through replication-transcription conflicts. *Nature*, **495**, 512–515.

42. Pomerantz,R.T. and O'Donnell,M. (2008) The replisome uses mRNA as a primer after colliding with RNA polymerase. *Nature*, **456**, 762–766.

43. Chen,Y.H., Keegan,S., Kahli,M., Tonzi,P., Fenyo,D., Huang,T.T. and Smith,D.J. (2019) Transcription shapes DNA replication initiation and termination in human cells. *Nat. Struct. Mol. Biol.*, **26**, 67–77.

44. Im,J.S., Keaton,M., Lee,K.Y., Kumar,P., Park,J. and Dutta,A. (2014) ATR checkpoint kinase and CRL1(beta TRCP) collaborate to degrade ASF1a and thus repress genes overlapping with clusters of stalled replication forks. *Gene. Dev.*, **28**, 875–887.

45. Goldknopf,I.L. and Busch,H. (1977) Isopeptide linkage between nonhistone and histone 2A polypeptides of chromosomal conjugate-protein A24. *Proc. Natl. Acad. Sci. USA*, **74**, 864–868.

46. Hunt,L.T. and Dayhoff,M.O. (1977) Amino-terminal sequence identity of ubiquitin and the nonhistone component of nuclear protein A24. *Biochem. Biophys. Res. Commun.*, **74**, 650–655.

47. Wang,H., Wang,L., Erdjument-Bromage,H., Vidal,M., Tempst,P., Jones,R.S. and Zhang,Y. (2004) Role of histone H2A ubiquitination in polycomb silencing. *Nature*, **431**, 873–878.

48. Bergink,S., Salomons,F.A., Hoogstraten,D., Groothuis,T.A.M., de Waard,H., Wu,J., Yuan,L., Citterio,E., Houtsmuller,A.B., Neefjes,J. *et al.* (2006) DNA damage triggers nucleotide excision repair-dependent monoubiquitylation of histone H2A. *Gene. Dev.*, **20**, 1343–1352.

49. Marteijn,J.A., Bekker-Jensen,S., Mailand,N., Lans,H., Schwertman,P., Gourdin,A.M., Dantuma,N.P., Lukas,J. and Vermeulen,W. (2009) Nucleotide excision repair-induced H2A ubiquitination is dependent on MDC1 and RNF8 and reveals a universal DNA damage response. *J Cell Biol*, **186**, 835–847.

50. Wu,J.X., Huen,M.S.Y., Lu,L.Y., Ye,L., Dou,Y.L., Ljungman,M., Chen,J.J. and Yu,X.C. (2009) Histone ubiquitination associates with BRCA1-Dependent DNA damage response. *Mol. Cell Biol.*, **29**, 849–860.

51. Zhu,Q.Z., Sharma,N., He,J.S., Wani,G. and Wani,A.A. (2015) USP7 deubiquitinase promotes ubiquitin-dependent DNA damage signaling by stabilizing RNF168*. *Cell Cycle*, **14**, 1413–1425.

52. Zhu,Q.Z., Wani,G., Arab,H.H., Ei-Mahdy,M.A., Ray,A. and Wani,A.A. (2009) Chromatin restoration following nucleotide

excision repair involves the incorporation of ubiquitinated H2A at damaged genomic sites. *DNA Repair*, **8**, 262–273.

53. Shanbhag,N.M., Rafalska-Metcalf,I.U., Balane-Bolivar,C., Janicki,S.M. and Greenberg,R.A. (2010) ATM-Dependent chromatin changes silence transcription in cis to DNA double-strand breaks. *Cell*, **141**, 970–981.

54. Zhao,M., Geng,R., Guo,X., Yuan,R., Zhou,X. and Zhong,Y. (2017) PCAF/GCN5-Mediated acetylation of RPA1 promotes nucleotide excision repair. *Cell Rep.*, **20**, 1997–2009.

55. Wang,H., Qiu,Z., Bo,L., Wu,Y., Ren,J., Liu,Y., Zhao,Y., Wang,Y., Hao,S. and Zheng,L. (2018) PLK1 targets CtIP to promote microhomology-mediated end joining. *Nucleic Acids Res.*, **46**, 10724–10739.

56. Wang,H., Shi,L.Z., Wong,C., Han,X., Hwang,Y.H., Truong,L.N., Zhu,Q., Shao,Z., Chen,D.J. and Berns,M.W. (2013) The interaction of CtIP and nbs1 connects CDK and ATM to regulate HR–Mediated double-strand break repair. *Plos Genetics*, **9**, e1003277.

57. Tian,T., Bu,M., Chen,X., Ding,L.L., Yang,Y.L., Han,J.H., Feng,X.H., Xu,P.L., Liu,T., Ying,S.M. *et al.* (2021) The ZATT-TOP2A-PICH axis drives extensive replication fork reversal to promote genome stability. *Mol. Cell*, **81**, 198–211.

58. Wang,H.L., Li,S.B., Oaks,J., Ren,J.P., Li,L. and Wu,X.H. (2018) The concerted roles of FANCM and rad52 in the protection of common fragile sites. *Nat. Commun.*, **9**, 2791.

59. Ling,H.B., Peng,L.R., Wang,J.B., Rahhal,R. and Seto,E. (2018) Histone deacetylase SIRT1 targets plk2 to regulate centriole duplication. *Cell Rep.*, **25**, 2851–2865.

60. Ui,A., Nagaura,Y. and Yasui,A. (2015) Transcriptional elongation factor ENL phosphorylated by ATM recruits polycomb and switches off transcription for DSB repair. *Mol. Cell*, **58**, 468–482.

61. Wang,H., Li,S., Oaks,J., Ren,J., Li,L. and Wu,X. (2018) The concerted roles of FANCM and rad52 in the protection of common fragile sites. *Nat. Commun.*, **9**, 2791.

62. Shechter,D., Dormann,H.L., Allis,C.D. and Hake,S.B. (2007) Extraction, purification and analysis of histones. *Nat. Protoc.*, **2**, 1445–1457.

63. Nieminuszczy,J., Schwab,R.A. and Niedzwiedz,W. (2016) The DNA fibre technique - tracking helicases at work. *Methods*, **108**, 92–98.

64. Ray Chaudhuri,A., Callen,E., Ding,X., Gogola,E., Duarte,A.A., Lee,J.E., Wong,N., Lafarga,V., Calvo,J.A., Panzarino,N.J. *et al.* (2016) Replication fork stability confers chemoresistance in BRCA-deficient cells. *Nature*, **535**, 382–387.

65. Sirbu,B.M., Couch,F.B. and Cortez,D. (2012) Monitoring the spatiotemporal dynamics of proteins at replication forks and in assembled chromatin using isolation of proteins on nascent DNA. *Nat. Protoc.*, **7**, 594–605.

66. Wang,H., Shi,L.Z., Wong,C.C., Han,X., Hwang,P.Y., Truong,L.N., Zhu,Q., Shao,Z., Chen,D.J., Berns,M.W. *et al.* (2013) The interaction of CtIP and nbs1 connects CDK and ATM to regulate HR-mediated double-strand break repair. *PLoS Genet*, **9**, e1003277.

67. Ren,J., Wu,Y., Wang,Y., Zhao,Y., Li,Y., Hao,S., Lin,L., Zhang,S., Xu,X. and Wang,H. (2021) CtIP suppresses primary microRNA maturation and promotes metastasis of colon cancer cells in a xenograft mouse model. *J. Biol. Chem.*, **296**, 100707.

68. Panneerselvam,J., Wang,H., Zhang,J., Che,R., Yu,H. and Fei,P. (2016) BLM promotes the activation of fanconi anemia signaling pathway. *Oncotarget*, **7**, 32351–32361.

69. Olive,P.L. and Banath,J.P. (2006) The comet assay: a method to measure DNA damage in individual cells. *Nat. Protoc.*, **1**, 23–29.

70. Agnese,C., Matthias,G., Kristiansen,M.S. and Natalia,G. (2018) RNA/DNA hybrid interactome identifies DXH9 as a molecular player in transcriptional termination and R-Loop-Associated DNA damage. *Cell Reports*, **23**, 1891–1905.

71. Tan,M., Luo,H., Lee,S., Jin,F., Yang,J.S., Montellier,E., Buchou,T., Cheng,Z., Rousseaux,S., Rajagopal,N. *et al.* (2011) Identification of 67 histone marks and histone lysine crotonylation as a new type of histone modification. *Cell*, **146**, 1016–1028.

72. Hu,J., Jing,H. and Lin,H. (2014) Sirtuin inhibitors as anticancer agents. *Future Med. Chem.*, **6**, 945–966.

73. Vigushin,D.M., Ali,S., Pace,P.E., Mirsaidi,N., Ito,K., Adcock,I. and Coombes,R.C. (2001) Trichostatin a is a histone deacetylase inhibitor with potent antitumor activity against breast cancer in vivo. *Clin. Cancer Res.*, **7**, 971–976.

74. Yang,X.J. and Seto,E. (2008) The rpd3/hda1 family of lysine deacetylases: from bacteria and yeast to mice and men. *Nat. Rev. Mol. Cell Biol.*, **9**, 206–218.

75. Ming,M., Shea,C.R., Guo,X., Li,X., Soltani,K., Han,W. and He,Y.Y. (2010) Regulation of global genome nucleotide excision repair by SIRT1 through xeroderma pigmentosum C. *Proc. Natl. Acad. Sci. USA*, **107**, 22623–22628.

76. Fan,W. and Luo,J. (2010) SIRT1 regulates UV-induced DNA repair through deacetylating XPA. *Mol. Cell*, **39**, 247–258.

77. Jeong,J., Juhn,K., Lee,H., Kim,S.H., Min,B.H., Lee,K.M., Cho,M.H., Park,G.H. and Lee,K.H. (2007) SIRT1 promotes DNA repair activity and deacetylation of Ku70. *Exp. Mol. Med.*, **39**, 8–13.

78. Yuan,Z., Zhang,X., Sengupta,N., Lane,W.S. and Seto,E. (2007) SIRT1 regulates the function of the nijmegen breakage syndrome protein. *Mol. Cell*, **27**, 149–162.

79. Mostoslavsky,R., Chua,K.F., Lombard,D.B., Pang,W.W., Fischer,M.R., Gellon,L., Liu,P., Mostoslavsky,G., Franco,S., Murphy,M.M. *et al.* (2006) Genomic instability and aging-like phenotype in the absence of mammalian SIRT6. *Cell*, **124**, 315–329.

80. Tang,M., Li,Z., Zhang,C., Lu,X., Tu,B., Cao,Z., Li,Y., Chen,Y., Jiang,L., Wang,H. *et al.* (2019) SIRT7-mediated ATM deacetylation is essential for its deactivation and DNA damage repair. *Sci. Adv.*, **5**, eaav1118.

81. Vaziri,H., Dessain,S.K., Ng Eaton,E., Imai,S.I., Frye,R.A., Pandita,T.K., Guarente,L. and Weinberg,R.A. (2001) hSIR2(SIRT1) functions as an NAD-dependent p53 deacetylase. *Cell*, **107**, 149–159.

82. Sparmann,A. and van Lohuizen,M. (2006) Polycomb silencers control cell fate, development and cancer. *Nat. Rev. Cancer.*, **6**, 846–856.

83. Di Croce,L. and Helin,K. (2013) Transcriptional regulation by polycomb group proteins. *Nat. Struct. Mol. Biol.*, **20**, 1147–1155.

84. Endoh,M., Endo,T.A., Endoh,T., Isono,K., Sharif,J., Ohara,O., Toyoda,T., Ito,T., Eskeland,R., Bickmore,W.A. *et al.* (2012) Histone H2A mono-ubiquitination is a crucial step to mediate PRC1-dependent repression of developmental genes to maintain ES cell identity. *PLoS Genetics*, **8**, e1002774.

85. Ginjala,V., Nacerddine,K., Kulkarni,A., Oza,J., Hill,S.J., Yao,M., Citterio,E., van Lohuizen,M. and Ganesan,S. (2011) BMI1 is recruited to DNA breaks and contributes to DNA damage-induced H2A ubiquitination and repair. *Mol. Cell. Biol.*, **31**, 1972–1982.

86. Ismail,I.H., Andrin,C., McDonald,D. and Hendzel,M.J. (2010) BMI1-mediated histone ubiquitylation promotes DNA double-strand break repair. *J. Cell Biol.*, **191**, 45–60.

87. Sanchez,A., De Vivo,A., Uprety,N., Kim,J., Stevens,S.M. Jr and Kee,Y. (2016) BMI1-UBR5 axis regulates transcriptional repression at damaged chromatin. *Proc. Natl. Acad. Sci. USA* , **113**, 11243–11248.

88. Neelsen,K.J. and Lopes,M. (2015) Replication fork reversal in eukaryotes: from dead end to dynamic response. *Nat. Rev. Mol. Cell Bio.*, **16**, 207–220.

89. Poole,L.A. and Cortez,D. (2017) Functions of SMARCAL1, ZRANB3, and HLTF in maintaining genome stability. *Crit. Rev. Biochem. Mol.*, **52**, 696–714.

90. Quinet,A., Lemacon,D. and Vindigni,A. (2017) Replication fork reversal: players and guardians. *Mol. Cell*, **68**, 830–833.

91. Schmid,J.A., Berti,M., Walser,F., Raso,M.C., Schmid,F., Krietsch,J., Stoy,H., Zwicky,K., Ursich,S., Freire,R. *et al.* (2018) Histone ubiquitination by the DNA damage response is required for efficient DNA replication in unperturbed s phase. *Mol. Cell*, **71**, 897–910.

92. Leung,K.H.T., Abou El Hassan,M. and Bremner,R. (2013) A rapid and efficient method to purify proteins at replication forks under native conditions. *Biotechniques*, **55**, 204–206.

93. Sirbu,B.M., Couch,F.B., Feigerle,J.T., Bhaskara,S., Hiebert,S.W. and Cortez,D. (2011) Analysis of protein dynamics at active, stalled, and collapsed replication forks. *Gene. Dev.*, **25**, 1320–1327.

94. Przetocka,S., Porro,A., Bolck,H.A., Walker,C., Lezaja,A., Trenner,A., von Aesch,C., Himmels,S.F., D'Andrea,A.D., Ceccaldi,R. *et al.* (2018) CtIP-Mediated fork protection synergizes with BRCA1 to suppress genomic instability upon DNA replication stress. *Mol Cell*, **72**, 568–582.

95. Salic,A. and Mitchison,T.J. (2008) A chemical method for fast and sensitive detection of DNA synthesis in vivo. *Proc. Natl. Acad. Sci. USA*, **105**, 2415–2420.

96. Betous,R., Mason,A.C., Rambo,R.P., Bansbach,C.E., Badu-Nkansah,A., Sirbu,B.M., Eichman,B.F. and Cortez,D. (2012) SMARCAL1 catalyzes fork regression and holliday junction migration to maintain genome stability during DNA replication. *Gene Dev.*, **26**, 151–162.

97. Blastyak,A., Hajdu,I., Unk,I. and Haracska,L. (2010) Role of double-stranded DNA translocase activity of human HLTF in replication of damaged DNA. *Mol Cell Biol*, **30**, 684–693.

98. Ciccia,A., Nimonkar,A.V., Hu,Y.D., Hajdu,I., Achar,Y.J., Izhar,L., Petit,S.A., Adamson,B., Yoon,J.C., Kowalczykowski,S.C. *et al.* (2012) Polyubiquitinated PCNA recruits the ZRANB3 translocase to maintain genomic integrity after replication stress. *Mol. Cell*, **47**, 396–409.

99. Zellweger,R., Dalcher,D., Mutreja,K., Berti,M., Schmid,J.A., Herrador,R., Vindigni,A. and Lopes,M. (2015) Rad51-mediated replication fork reversal is a global response to genotoxic treatments in human cells. *J. Cell Biol.*, **208**, 563–579.

100. Schlacher,K., Christ,N., Siaud,N., Egashira,A., Wu,H. and Jasin,M. (2011) Double-Strand break repair-independent role for BRCA2 in blocking stalled replication fork degradation by MRE11. *Cell*, **145**, 529–542.

101. Schlacher,K., Wu,H. and Jasin,M. (2012) A distinct replication fork protection pathway connects fanconi anemia tumor suppressors to RAD51-BRCA1/2. *Cancer Cell*, **22**, 106–116.

102. Sanchez,A., de Vivo,A., Tonzi,P., Kim,J., Huang,T.T. and Kee,Y. (2020) Transcription-replication conflicts as a source of common fragile site instability caused by BMI1-RNF2 deficiency. *PLoS Genetics*, **16**, e1008524.

103. Okamoto,Y., Abe,M., Itaya,A., Tomida,J., Ishiai,M., Takaori-Kondo,A., Taoka,M., Isobe,T. and Takata,M. (2019) FANCD2 protects genome stability by recruiting RNA processing enzymes to resolve R-loops during mild replication stress. *FEBS J.*, **286**, 139–150.

104. Boguslawski,S.J., Smith,D.E., Michalak,M.A., Mickelson,K.E., Yehle,C.O., Patterson,W.L. and Carrico,R.J. (1986) Characterization of monoclonal-antibody to DNA.Rna and its application to immunodetection of hybrids. *J. Immunol. Methods*, **89**, 123–130.

105. Zhu,Q., Pao,G.M., Huynh,A.M., Suh,H., Tonnu,N., Nederlof,P.M., Gage,F.H. and Verma,I.M. (2011) BRCA1 tumour suppression occurs via heterochromatin-mediated silencing. *Nature*, **477**, 179–184.

106. Densham,R.M., Garvin,A.J., Stone,H.R., Strachan,J., Baldock,R.A., Daza-Martin,M., Fletcher,A., Blair-Reid,S., Beesley,J., Johal,B. *et al.* (2016) Human BRCA1-BARD1 ubiquitin ligase activity counteracts chromatin barriers to DNA resection. *Nat. Struct. Mol. Biol.*, **23**, 647–655.

107. Im,J.S., Keaton,M., Lee,K.Y., Kumar,P., Park,J. and Dutta,A. (2014) ATR checkpoint kinase and CRL1betaTRCP collaborate to degrade ASF1a and thus repress genes overlapping with clusters of stalled replication forks. *Genes. Dev.*, **28**, 875–887.

108. Kile,A.C., Chavez,D.A., Bacal,J., Eldirany,S., Korzhnev,D.M., Bezsonova,I., Eichman,B.F. and Cimprich,K.A. (2015) HLTF's ancient HIRAN domain binds 3 ' DNA ends to drive replication fork reversal. *Mol Cell*, **58**, 1090–1100.

109. Kolinjivadi,A.M., Sannino,V., De Antoni,A., Zadorozhny,K., Kilkenny,M., Techer,H., Baldi,G., Shen,R., Ciccia,A., Pellegrini,L. *et al.* (2017) Smarcal1-Mediated fork reversal triggers mre11-dependent degradation of nascent DNA in the absence of brca2 and stable rad51 nucleofilaments. *Mol. Cell*, **67**, 867–881.

110. Lemacon,D., Jackson,J., Quinet,A., Brickner,J.R., Li,S., Yazinski,S., You,Z.S., Ira,G., Zou,L., Mosammaparast,N. *et al.* (2017) MRE11 and EXO1 nucleases degrade reversed forks and elicit MUS81-dependent fork rescue in BRCA2-deficient cells. *Nat. Commun.*, **8**, 860.

111. Mijic,S., Zellweger,R., Chappidi,N., Berti,M., Jacobs,K., Mutreja,K., Ursich,S., Chaudhuri,A.R., Nussenzweig,A., Janscak,P. *et al.* (2017) Replication fork reversal triggers fork degradation in BRCA2-defective cells. *Nat Commun*, **8**, 859.

112. Wei,W., Liu,X., Chen,J., Gao,S., Lu,L., Zhang,H., Ding,G., Wang,Z., Chen,Z., Shi,T. *et al.* (2017) Class i histone deacetylases are major histone decrotonylases: evidence for critical and broad function of histone crotonylation in transcription. *Cell Res.*, **27**, 898–915.